

High-lift aerodynamics

Objectives of high-lift systems

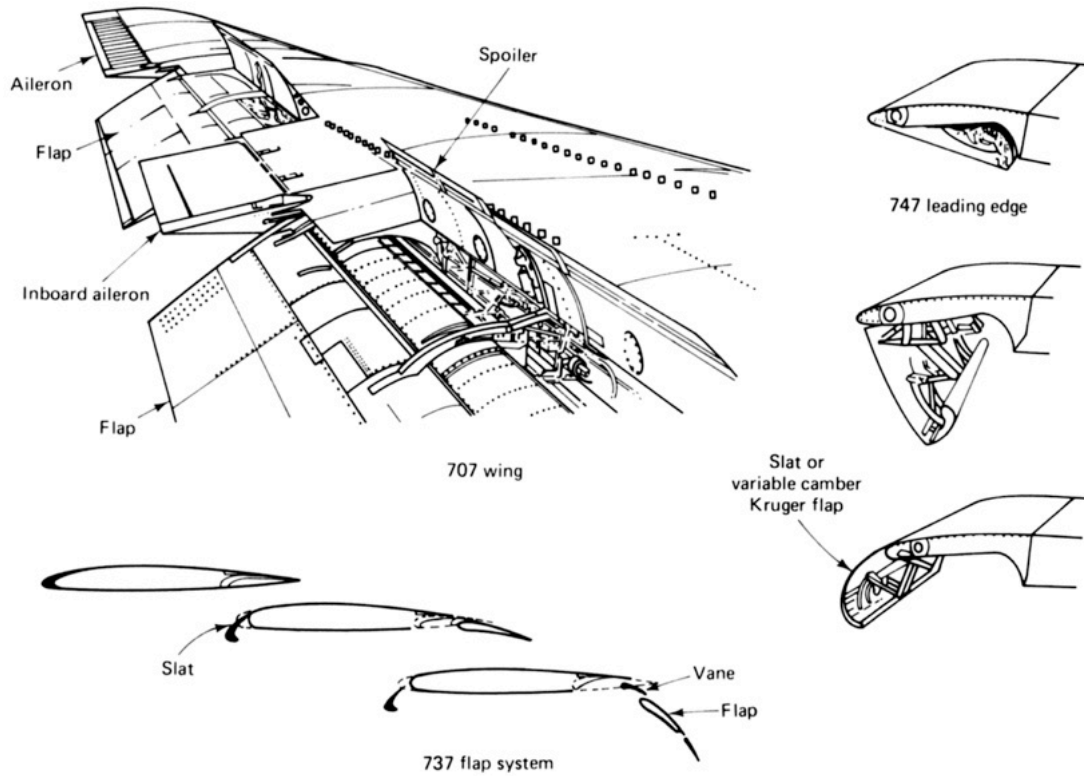


747 high-lift system at touchdown.

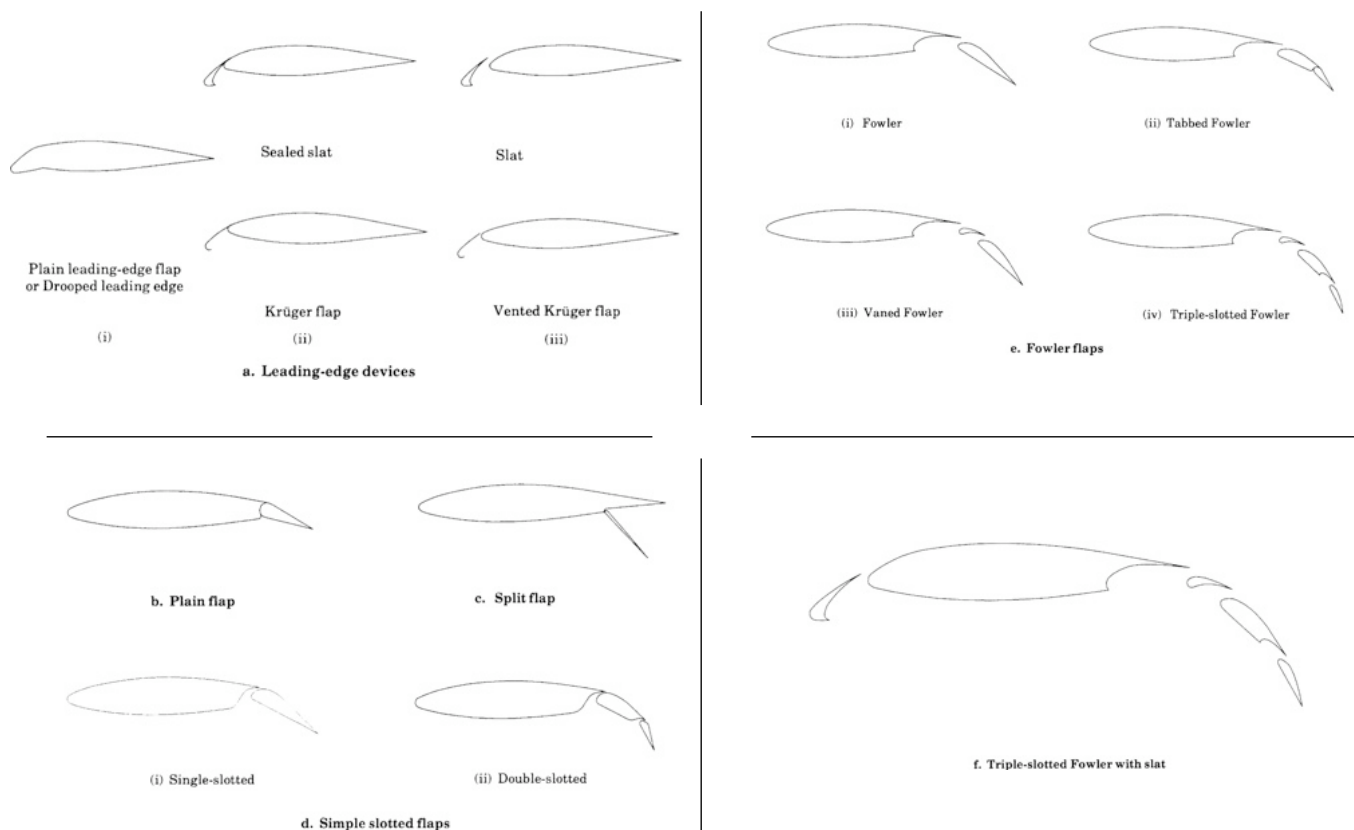
1. Obtain the highest C_{lmax} , to obtain slowest approach speed and minimum runway length at landing.
2. Get the maximum ratio L/D at takeoff, to maximize climb angle (jet) or rate of climb (prop)
— $C_l \approx 0.7-0.8 C_{lmax}$.
3. Develop a reasonably high drag at landing to help reduce speed and increase glide slope.

These requirements mean that it is now almost mandatory to use variable airfoil geometry and/or multi-element airfoils in high-lift systems. In the latter case we still want to achieve the highest C_{lmax} for each component.

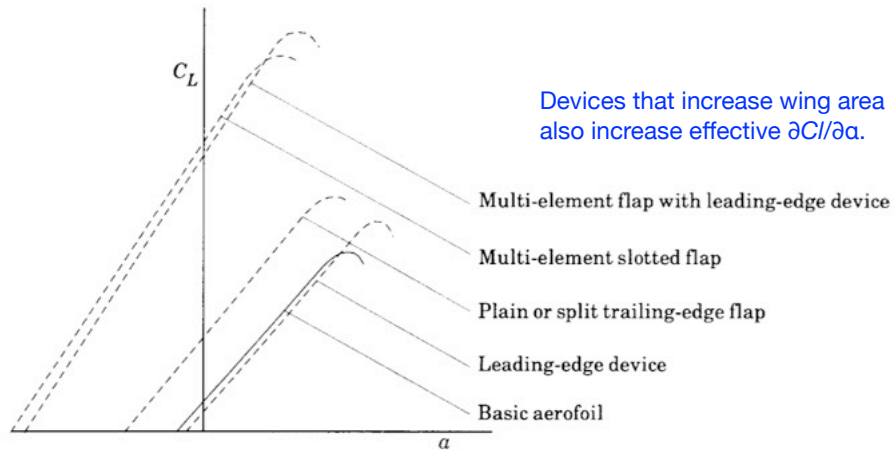
Elements of common high-lift systems



High lift devices (multi-component airfoils) — 2



High lift devices (multi-component airfoils) — 3



Devices that increase camber at TE reduce α_0 .

Devices that increase camber at LE increase α_0 .

High-Lift Device		Typical Flap Angle		$(C_L)_{\max} / \cos \Lambda$	
Trailing Edge	Leading Edge	Takeoff	Landing	Takeoff	Landing
Plain flap		20°	60°	1.4–1.6	1.7–2.0
Single-slotted flap		20°	40°	1.5–1.7	1.8–2.2
Fowler flap					
single-slotted		15°	40°	2.0–2.2	2.5–2.9
double-slotted		20°	50°	1.7–1.95	2.3–2.7
double-slotted	slat	20°	50°	2.3–2.6	2.8–3.2
triple-slotted	slat	20°	40°	2.4–2.7	3.2–3.5

Λ is the $c/4$ wing sweep angle.

More complicated and larger high-lift systems can increase $C_{L\max}$ but also cost more in terms of weight, maintenance and purchase price.

A less obvious effect is that they also tend to reduce available fuel volume.

Airfoil high-lift system basics

There are three effects that determine the increase in lift achieved:

1. An increase in camber
2. An increase in effective chord
3. The mutual interaction effect of separated components

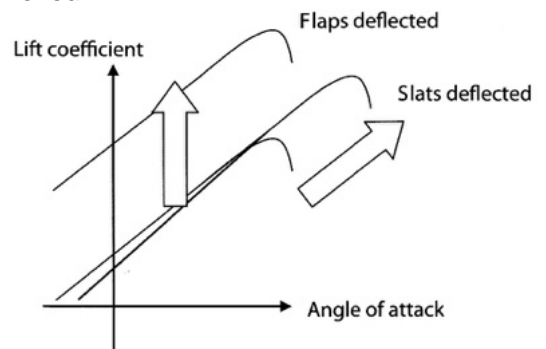


Figure 25.1 - Effect of flaps and slats on the lift curve

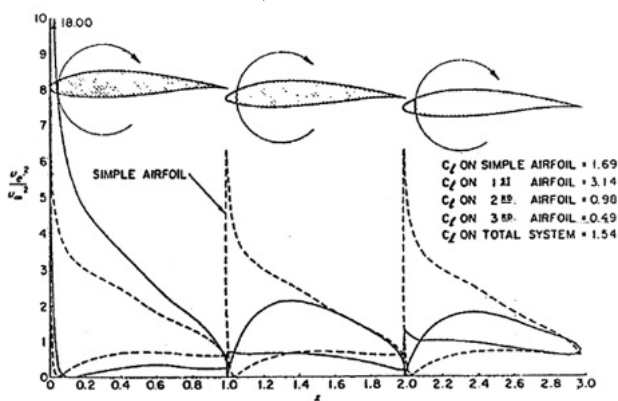


Figure 25.3 - Pressure distribution on a three-element airfoil formed by NACA 63-, 615 sections arranged as shown, all three at $\alpha = 10^\circ$. Also shown is the pressure distribution on the basic single section. The slot gaps are 1% of the basic section chord. Source: AIAA Paper No. 74-939 High-lift Aerodynamics, A.M.O. Smith.

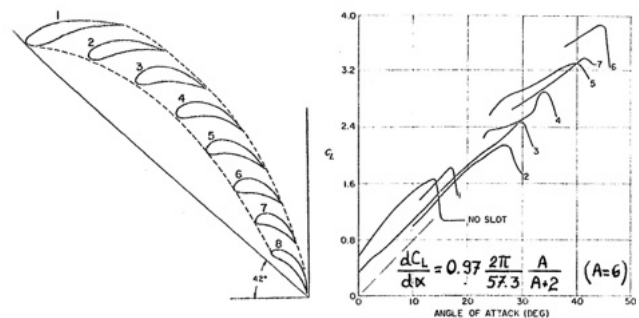
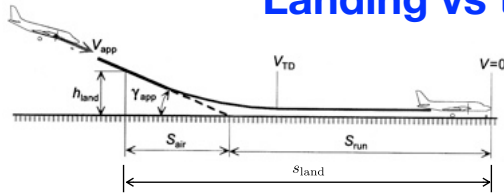


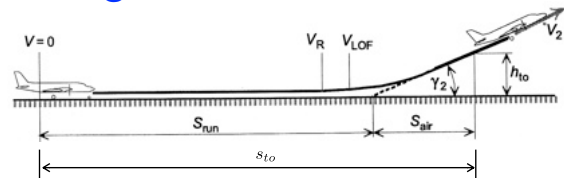
Figure 25.5 - A multi-component airfoil section within the contour of a modified RAF 19 airfoil section. Source: AIAA Paper No. 74-939

Figure 25.6 - Lift curves of the section of figure 25.5 with a successively increasing number of gaps between the components. Source: AIAA Paper No. 74-939

Landing vs take-off configuration



$$s_{\text{land}} \approx \frac{h_{\text{land}}}{\tan \gamma_{\text{app}}} + 1.69 \frac{W/S}{\rho |\bar{a}| C_{L,\text{max}}}$$



$$s_{\text{to}} \approx \frac{1}{\rho g r_T} \frac{1}{C_{L_2}} \frac{W}{S} \frac{W}{T_{\text{to}}} + \frac{h_{\text{to}}}{T_2/W - (C_D/C_L)_2}$$

Recall that performance considerations in landing and take-off segments are somewhat different.

In landing one is largely concerned with slow speed/ground roll and most attention goes to $C_{L,\text{max}}$.

In takeoff one is concerned with both with ground roll AND climb rate – attention goes to optimising a combination involving both C_L and L/D .

Hence one typically sees a different deployment of the same high-lift system for the two segments.

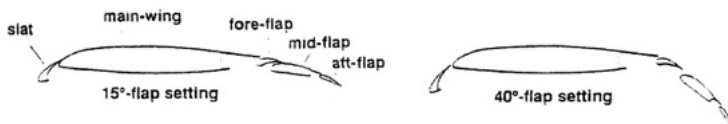


Figure 25.10 – Slat and flap positions at mid-semi-span for take-off and landing of the Boeing 737.
Source: AIAA Paper No. 93-3140

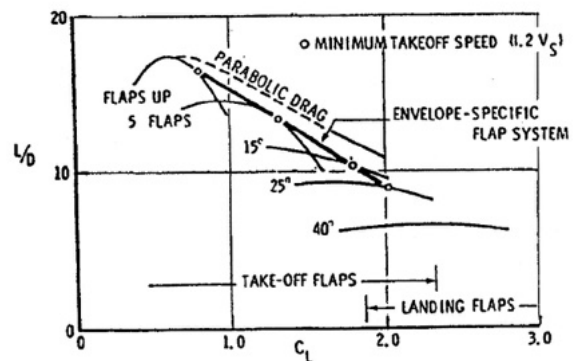


Figure 27.4 - Take-off aerodynamics, polar envelope.
Source: Shell Aviation News nos. 343, 344 / AIAA Paper No 65-739

Design of high lift devices

To achieve highest lift:

1. Lift should be as evenly distributed as possible for a given peak suction in each component.
2. Avoid excessive (adverse) pressure gradients by design of geometry and/or BL control.
3. Extend multicomponent airfoil chord.
4. Keep peak nose suction relatively low.
5. Increase lift over mid and aft sections of multicomponent airfoil.
6. Add fresh air to the BL behind peak suction.

Nose peak suction is controlled by:

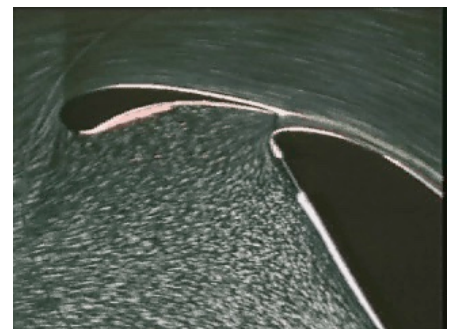
1. Nose radius and camber.
2. LE devices — flaps, slots, slats.

LE devices suppress the suction peak over the LE and reduce the likelihood of LE separation at high α . They act by:

1. Camber changes: nose and Kruger flaps, or
2. Improving BL energy: LE slots and slats (most effective).

Lift over mid and aft sections is controlled by:

1. Camber changes (reduces α_0).
2. Flap systems that improve BL energy: slotted flaps.



BL energy improvement is achieved through slots that bring energy from lower to upper surface.

Why is C_{Lmax} prediction so difficult?

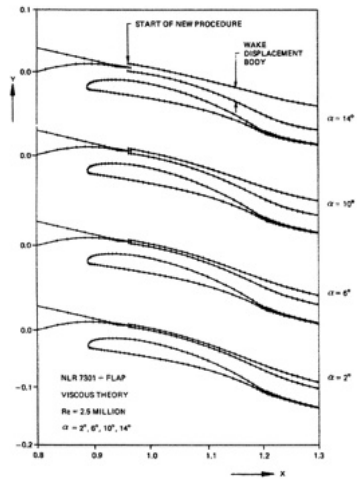
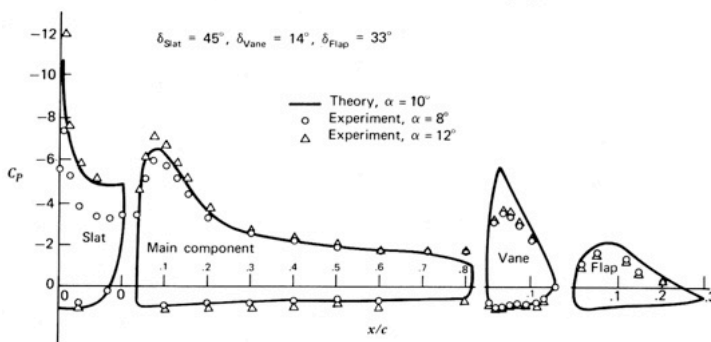
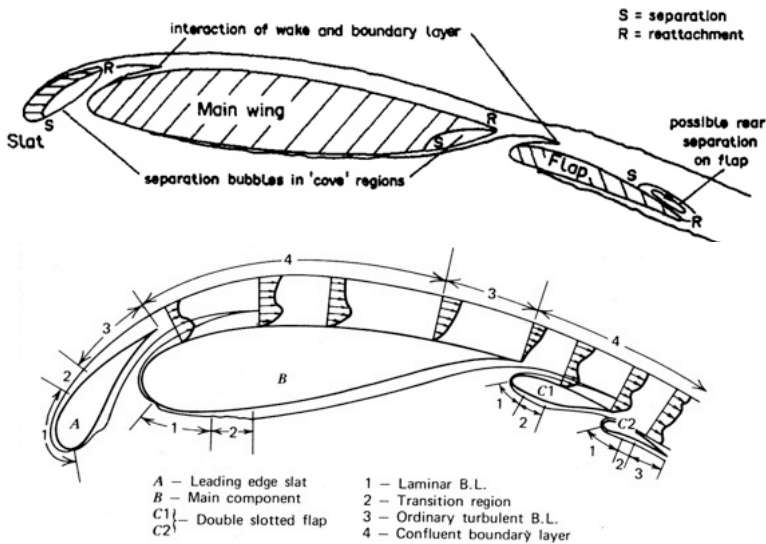


Figure 25.28 - Growth in wing-wake displacement body with increasing angle-of-attack in theoretical viscous flow. Source: AGARD CP-365, Paper No.3

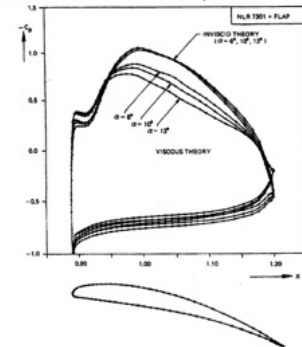


Figure 25.30 - Theoretical pressure distribution on the flap in inviscid and in viscous flow for $\alpha = 6, 10$ and 13 deg. Source: AGARD CP-365, Paper No. 3.

Possible flow separation/stall mechanisms

With a number of different lifting components interacting, a variety of possible flow separation locations arise:

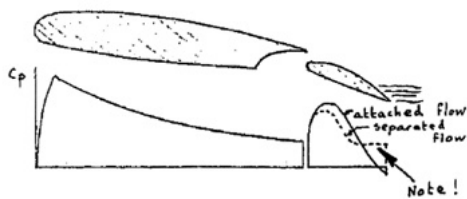


Figure 25.14 - Trailing edge stall on the flap for a section without a slat

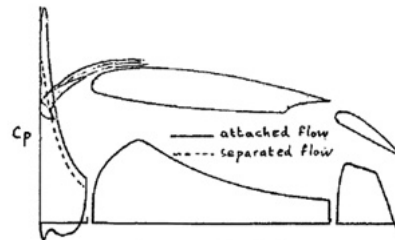


Figure 25.17 - Stall on the slat

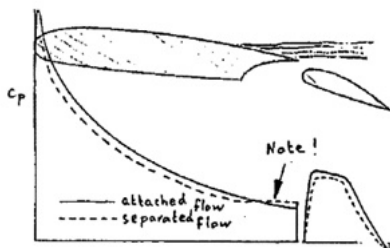


Figure 25.15 - Trailing edge stall on the main component for a section without a slat

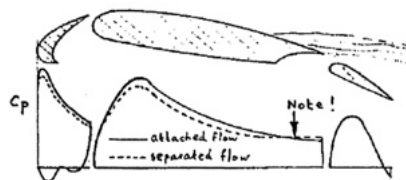


Figure 25.18 - Trailing-edge stall on the main component for a section with a slat

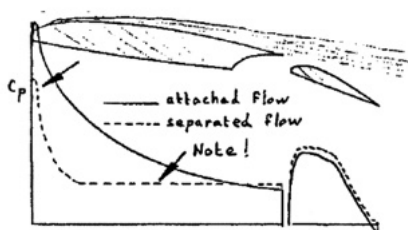


Figure 25.16 - Leading-edge stall on the main component for a section without a slat.

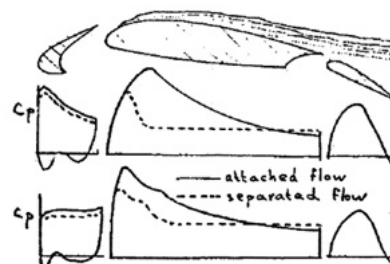


Figure 25.19 - Leading-edge stall on the main component for a section with a slat

Introduction to published design guides - ESDU

Engineering Sciences Data Unit — 1

	Go	About us	Products	Sectors	Support	Contact Us
--	----	----------	----------	---------	---------	------------

Search: [?] [+]


Go


ESDU Explorer


- Aerodynamics
- Aircraft Noise
- Composites
- Dynamics
- Fatigue - Endurance Data
- Fatigue - Fracture Mechanics
- Fluid Mechanics, Internal Flow
- Fluid Mechanics, Internal Flow (Aerospace)
- Heat Transfer
- Mechanisms
- Metallic Materials Data Handbook (MMDH)
- Performance
- Physical Data, Chemical Engineering
- Stress and Strength
- Structures
- Transonic Aerodynamics
- Tribology
- Vibration and Acoustic Fatigue
- Wind Engineering

ESDU - For engineers by engineers

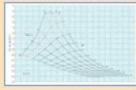
Expedite your design process with confidence using ESDU - a hands-on, practical engineering tool for arriving at the best design solution in the least amount of time.

→ Aerospace



→ Energy


→ Academic



ESDU provides validated engineering design data, methods and software that form an important part of the design process for industry professionals. The ESDU collection allows you to explore and optimise design iterations so you can validate your final design quicker and easier.




As part of our process of continuous improvement to ESDU's product offering, and our focus on improving customer satisfaction, ESDU is pleased to announce the introduction of Interactive Graphs...



To learn more about ESDU, and gain a better understanding of how ESDU can help your design and analysis, view an ESDU product demo.



The ESDU Engineering Service.
As part of your subscription you may communicate directly with our engineers by using the ESDU Engineering Service.



ESDU is a fundamental learning and teaching tool for Faculty and Students. The ESDU Academic site is an industrially relevant resource, providing empirical and theoretical methods, worked examples and software.

Engineering Sciences Data Unit — 2



ESDU Aerospace

Contents

Summary

Aerospace documents and software

Aerodynamics

Aircraft Noise

Composites

Dynamics

Fatigue - Endurance Data

Fatigue - Fracture Mechanics

Fluid Mechanics, Internal Flow (Aerospace)

Heat Transfer

Performance

Stress and Strength

Structures

Transonic Aerodynamics

Vibration and Acoustic Fatigue

Engineering Sciences Data Unit — 3



ESDU Aerospace
- Aerodynamics

[+] GENERAL - Organisation, properties of gases, isentropic flow and shock waves.

[+] GENERAL - Properties of the atmosphere

[+] GENERAL - Wind speeds and atmospheric turbulence

[+] AEROFOILS AND WINGS - General. Aerofoils at subcritical speeds - lift, pitching moment.

[+] AEROFOILS AND WINGS - Aerofoils at subcritical speeds - drag.

[+] AEROFOILS AND WINGS - Aerofoils at supersonic speeds. Critical Mach number and pressure coefficient. Flat plates.

[+] AEROFOILS AND WINGS - Wings - lift, pitching moment, aerodynamic centre, spanwise loading

[+] AEROFOILS AND WINGS - Wings - lift, pitching moment, aerodynamic centre, spanwise loading (continued)

[+] AEROFOILS AND WINGS - Wings - drag

[+] BODIES - General

[+] BODIES - Drag

[+] BODIES - Drag (continued)

[+] BODIES - Pressure distribution, normal force, pitching moment, centre of pressure.

[+] WING-BODY COMBINATIONS - Lift, normal force, pitching moment, aerodynamic centre, upwash

[+] WING-BODY COMBINATIONS - Lift, normal force, pitching moment, aerodynamic centre, upwash (continued). Drag.

[+] CONTROLS AND FLAPS - Controls - lift, pitching moment, rolling moment, drag

[+] CONTROLS AND FLAPS - Controls - hinge moment

[+] CONTROLS AND FLAPS - Flaps - lift: aerofoils

[+] CONTROLS AND FLAPS - Flaps - lift: wings.

[+] CONTROLS AND FLAPS - Flaps - lift curve. Flaps - drag.

[+] CONTROLS AND FLAPS - Flaps - pitching moment.

[+] EXCRESCENCE DRAG - Excrescence drag

[+] EXCRESCENCE DRAG - Excrescence drag (continued)

[+] CAVITY DRAG. UNDERCARRIAGE DRAG. CANOPY DRAG. - Cavity drag Undercarriage drag Canopy drag.

[+] CAVITY AERODYNAMICS AND AERO-ACOUSTICS - Cavity aerodynamics and aero-acoustics.

[+] INTERNAL FLOW SYSTEMS - Ducts, nacelles, intakes, nozzles

[+] INTERNAL FLOW SYSTEMS - Nacelles, intakes and nozzles (continued).

[+] POWERPLANT/AIRFRAME INTERACTIONS - Propeller powered aircraft

[+] POWERPLANT/AIRFRAME INTERACTIONS - Propeller powered aircraft (continued), jet powered aircraft

[+] STABILITY OF AIRCRAFT - General. Longitudinal stability.

[+] STABILITY OF AIRCRAFT - Longitudinal stability - derivatives due to rate of pitch. Pitch-break characteristics.

[+] STABILITY OF AIRCRAFT - Lateral stability - derivatives due to sideslip

[+] STABILITY OF AIRCRAFT - Lateral stability - derivatives due to sideslip (continued)

[+] STABILITY OF AIRCRAFT - Lateral stability - derivatives due to rate of roll, derivatives due to rate of yaw

[+] UNSTEADY AERODYNAMICS - Unsteady aerodynamics

[+] BLUFF BODIES AND STRUCTURES - Mean forces.

[+] BLUFF BODIES AND STRUCTURES - Fluctuating forces and response.

[+] AERODYNAMIC HEATING AND HEAT TRANSFER - Aerodynamic heating and heat transfer.

[+] WIND-TUNNEL CORRECTIONS - Wind-tunnel corrections.

[+] AERODYNAMICS SOFTWARE.

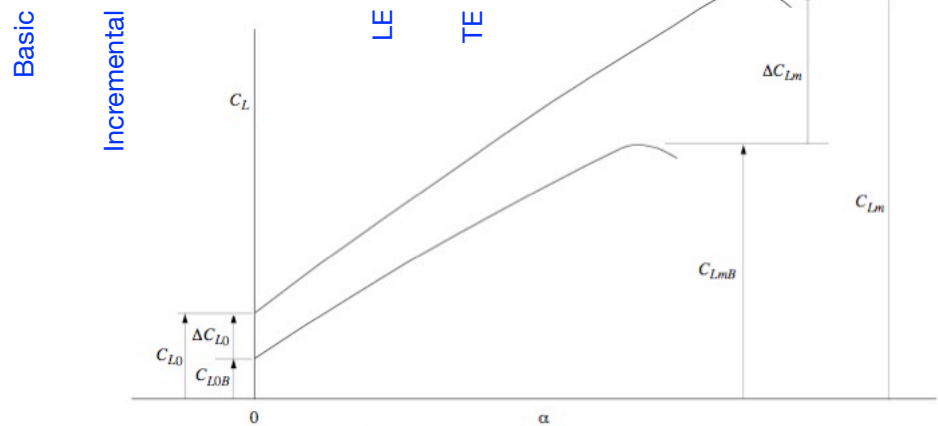
ESDU method for estimation of C_{lmax} at low speeds

Topics:

- Effects of LE devices and TE flaps.
- C_l vs α for a single airfoil.
- C_l vs α for various devices
 - LE device
 - TE flap
- Experimental evidence of range of applicability.

$$\alpha=0 \quad C_{L0} = C_{L0B} + \Delta C_{L0} = C_{L0B} + \Delta C_{L0l} + \Delta C_{L0t} \quad (3.1)$$

$$\max \quad C_{Lm} = C_{LmB} + \Delta C_{Lm} = C_{LmB} + \Delta C_{Lml} + \Delta C_{Lmt} \quad (3.2)$$



Sketch 3.1 Build up of C_{L0} and C_{Lm} for aerofoils

ESDU method for estimation of C_{lmax} at low speeds

TABLE 3.1 Locations of information for determination of C_{L0} and C_{Lm} for aerofoils

High-lift devices		Data Provided	Item No.	Reference No.
Leading-edge	Trailing-edge			
none	none	C_{L0B}, C_{LmB}	84026	16
any	none	$\Delta C_{L0l}, \Delta C_{Lml}$	94027	26
none	plain	$\Delta C_{L0t}, \Delta C_{Lmt}$	94028	27
	split		94029	28
	single-slotted		94030	29
	double-slotted		94031	30
	triple-slotted		94031	30
any	plain	$\Delta C_{L0}, \Delta C_{Lm}$	94028	27
	split		94029	28
	single-slotted		94027, 94030	26, 29
	double-slotted		94031	30
	triple-slotted		94031	30

An introduction to the characteristics of aerofoils with high-lift devices deployed is given in Item No. 94026 (Reference 25).

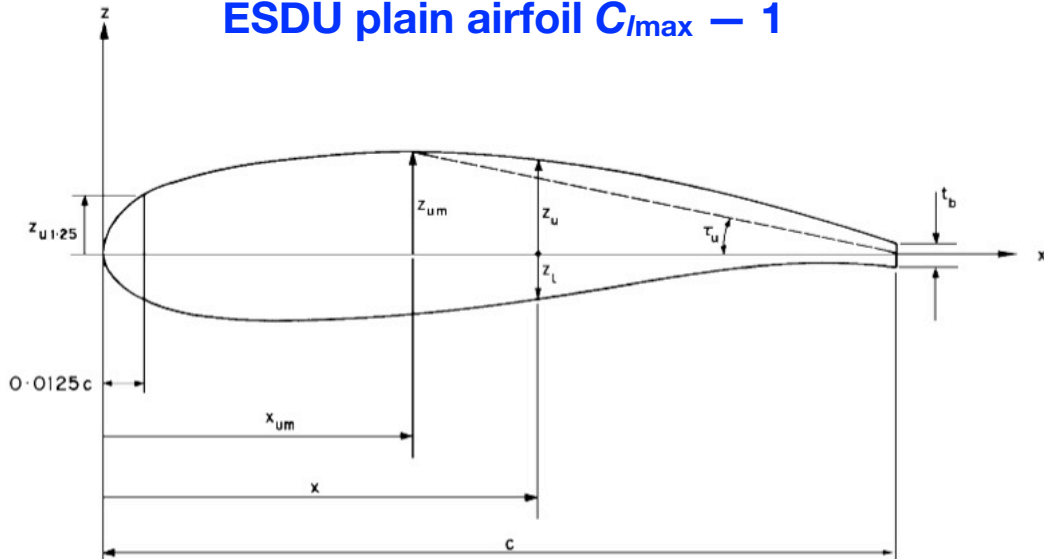
Basic

LE only

TE only

Combination

ESDU plain airfoil $C_{l_{\max}}$ — 1



The aerofoil maximum lift coefficient is obtained as follows:

$$C_{Lm} = (C_{L0} + \Delta C_L) F_S F_M \quad (2.1)$$

in which the increment ΔC_L is obtained from Section 3 or 4 and C_{L0} is obtained from Section 5. For modern aerofoils the factor F_S is obtained from Section 6 while for conventional sections $F_S = 1.0$. The factor F_M , obtained from Section 7, allows for the effect of Mach number up to 0.4. For $M \leq 0.1$, $F_M = 1.0$.

So we need C_{l0} and ΔC_l , as well as F_S and F_M .

(‘Modern aerofoils’ are those with large rear camber.)

ESDU plain airfoil $C_{l_{\max}}$ — 2

5. LIFT COEFFICIENT AT ZERO INCIDENCE

The coefficient C_{L0} for use in Equation (2.1) is obtained by combining the lift-curve slope, $(a_1)_0$, for incompressible flow obtained from Item No. Aero W 01.01.05 (Reference 21) with the zero-lift angle, α_0 , obtained by use of Pankhurst’s method in Derivation 1,

$$\alpha_0 = -\frac{\pi}{90} \sum_{i=1}^{14} (B_i z_{ci}/c), \quad (5.1) \quad \alpha_0 \text{ in radians}$$

$$\text{where} \quad z_{ci} = [z_u(x_i/c) + z_l(x_i/c)]/2. \quad (5.2)$$

The coefficients B_i are specified in Table 5.1 for the required values of x_i/c .

TABLE 5.1
Coefficients B_i in Equation (5.1)

i	x_i/c	B_i	i	x_i/c	B_i
1*	0	1.45	8	0.50	3.67
2	0.025	2.11	9	0.60	4.69
3	0.05	1.56	10	0.70	6.72
4	0.10	2.41	11	0.80	11.75
5	0.20	2.94	12	0.90	21.72
6	0.30	2.88	13	0.95	99.85
7	0.40	3.13	14*	1.0	-164.88

* Note that for the present definition of chord line the terms $i = 1$ and 14 do not contribute to α_0 .

Hence, the lift coefficient at zero incidence ($\alpha = 0$) is given by

$$C_{L0} = -\alpha_0 (a_1)_0. \quad (5.3)$$

Next we need $(a_1)_0$, the lift curve slope at $\alpha=0$ (approx. $2\pi/\text{rad.}$)

ESDU plain airfoil C_{lmax} — 3

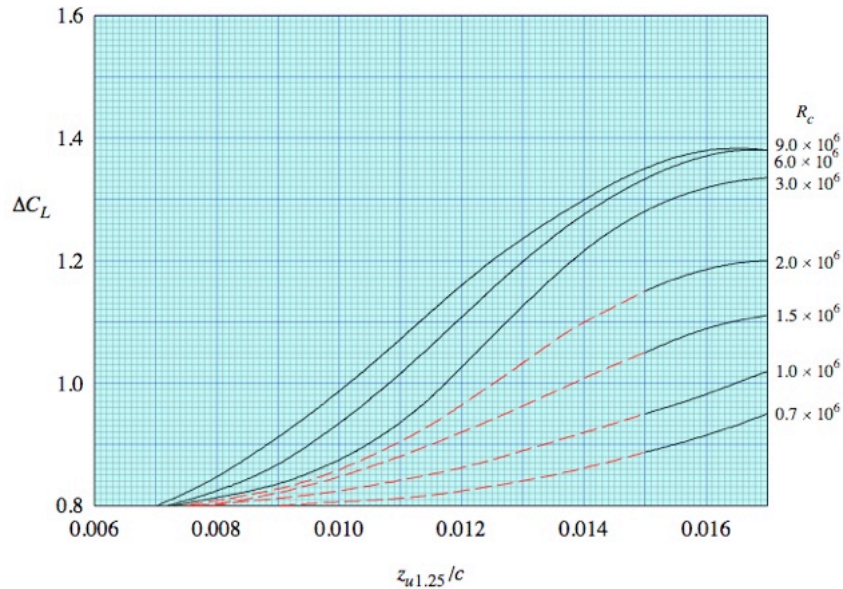
Derivation 2 gives the following equations representing Figures 1 to 3:

$$\frac{(a_1)_0}{(a_1)_{0T}} = 1 - \frac{0.1 + (1.05 - 0.5 x_t/c) \tan(\frac{1}{2}\tau_a)}{(\log_{10} R - 5)^{[1 - 2.5 \tan(\frac{1}{2}\tau_a)]}} \quad \tan(\tau_a/2) = \frac{t_{0.9} - t_{0.99}}{0.18c} \quad (2.1)$$

for Figures 1 and 2, where x_t/c is the boundary layer transition location,

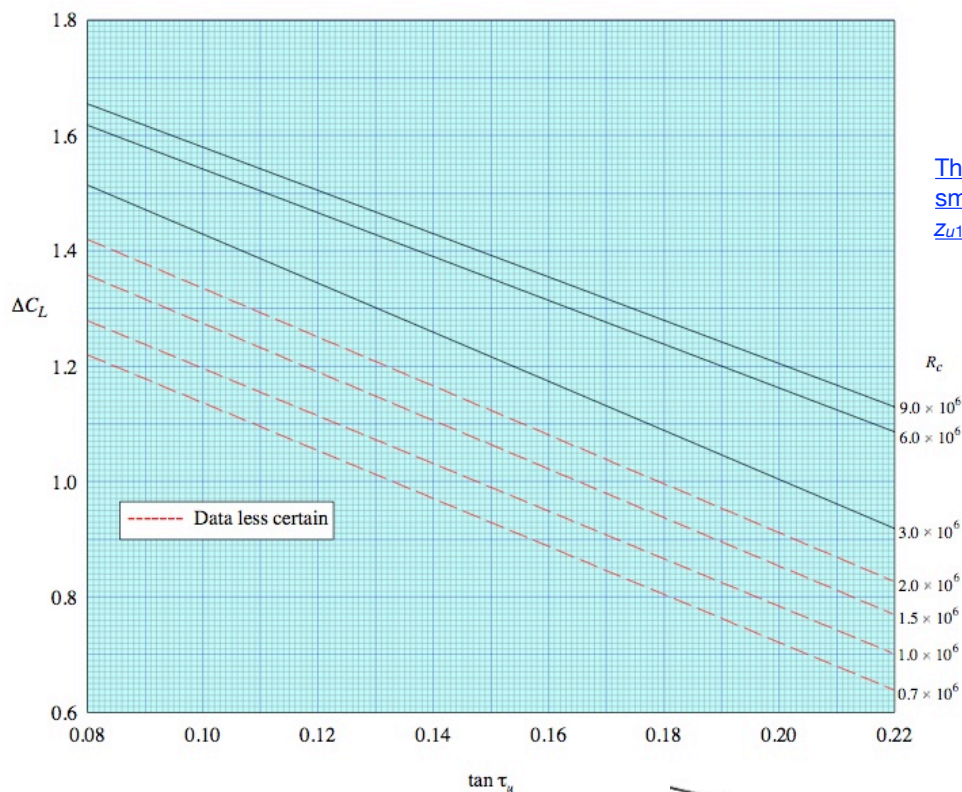
and $(a_1)_{0T} = 2\pi + (4.75 + 0.02\tau) t/c \quad \tau \approx \tau_a \quad (2.2)$

Now we have C_{l0} . Next we need ΔC_{li} .



These data for smooth airfoils with $z_{u1.25}/c < 0.017$

ESDU plain airfoil C_{lmax} — 4



These data for smooth airfoils with $z_{u1.25}/c > 0.017$

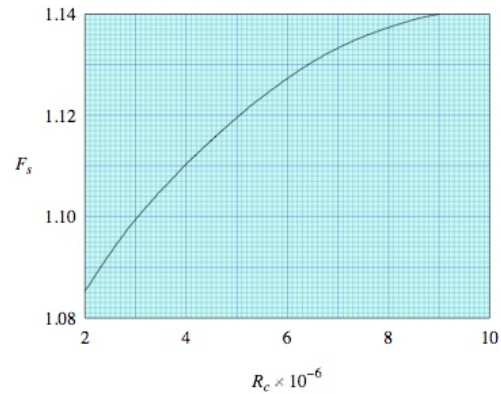
recall



ESDU plain airfoil C_{lmax} — 5

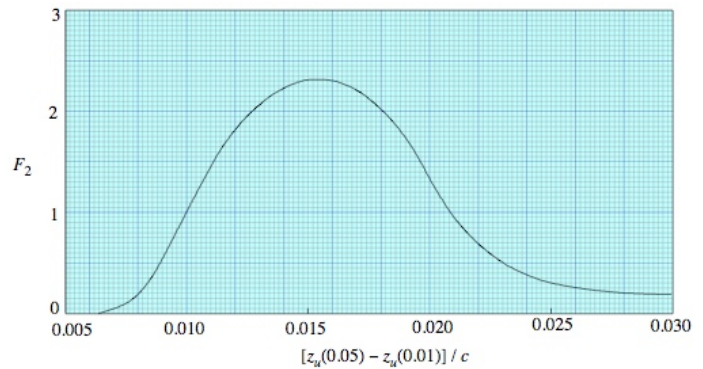
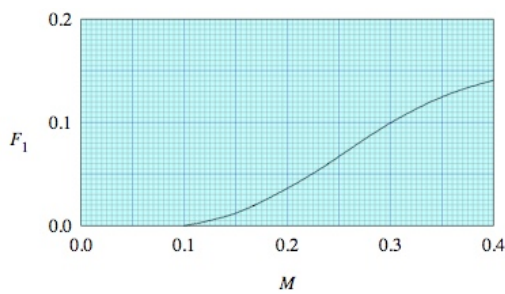
Finally we need correction factors F_S and F_M .

F_S (section) accounts for increase in C_{lmax} for modern sections with significant rear camber, otherwise $F_S=1$.



F_M (Mach number) accounts for reduction in C_{lmax} with M , most significant for sections with small nose radius,

$$F_M = 1 - F_1 F_2$$



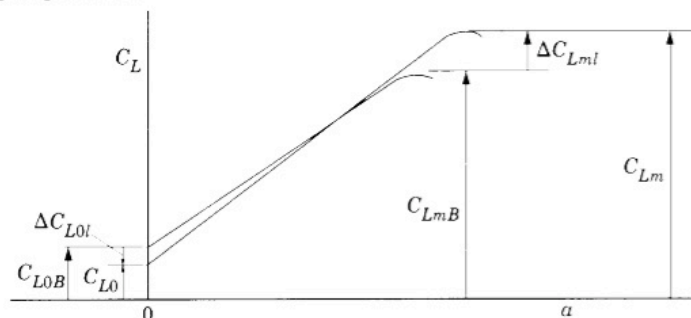
ESDU LE, TE device effects on C_{lmax}

Recall

$$C_{L0} = C_{L0B} + \Delta C_{L0} = C_{L0B} + \Delta C_{L0l} + \Delta C_{L0t} \quad \text{where } l \Rightarrow \text{LE device}$$

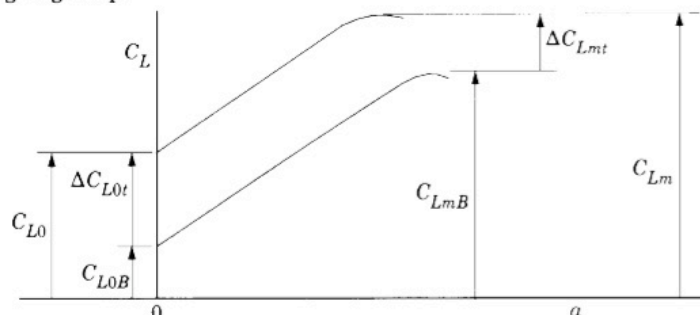
$$C_{Lm} = C_{LmB} + \Delta C_{Lm} = C_{LmB} + \Delta C_{Lml} + \Delta C_{Lmt} \quad \text{where } t \Rightarrow \text{TE device}$$

a. Leading-edge device



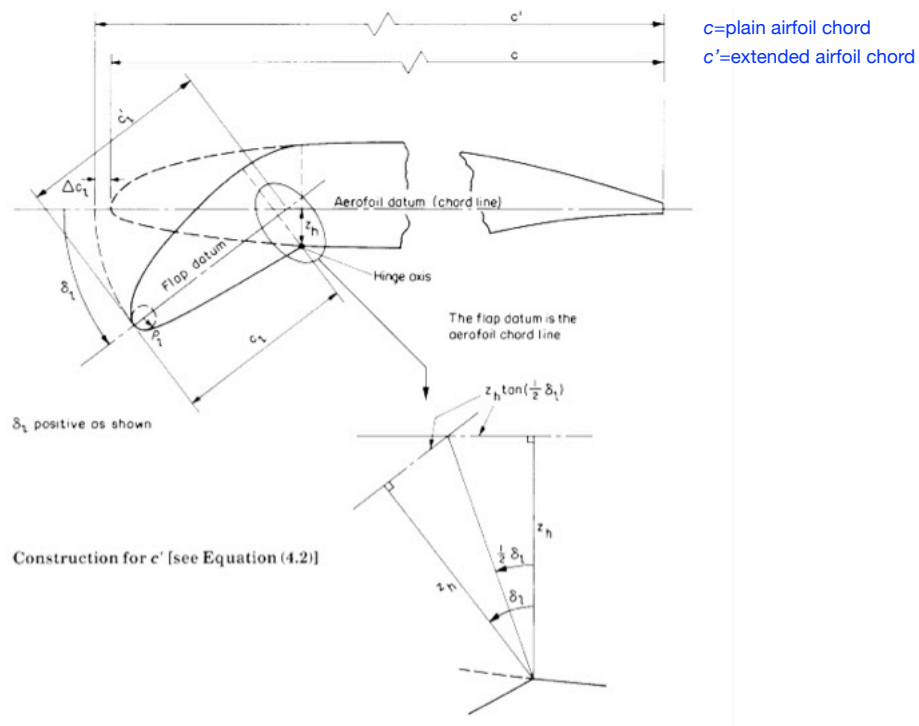
Note ΔC_{L0l} is negative because zero-lift α increases with device deployment.

b. Trailing-edge flap



ESDU LE device effects on C_{lmax} — 1

c_l =chord of LE device
 c_l' =extended chord of LE device
 Δc_l =chord extension due to deployment of LE device



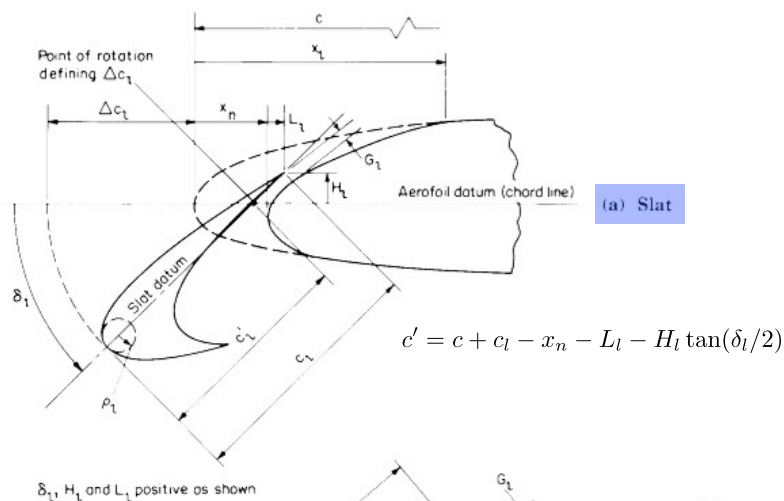
Sketch 4.1 Plain leading-edge flaps and drooped leading edges

From Sketch 4.1,

$$c_l' = c_l + z_h \tan(\delta_l/2) \quad (4.1)$$

and
$$c' = c + 2z_h \tan(\delta_l/2). \quad (4.2)$$

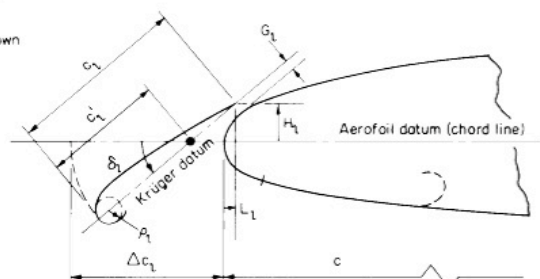
ESDU LE device effects on C_{lmax} — 2



$$c' = c + c_l - x_n - L_l - H_l \tan(\delta_l/2)$$

δ_l , H_l and L_l positive as shown

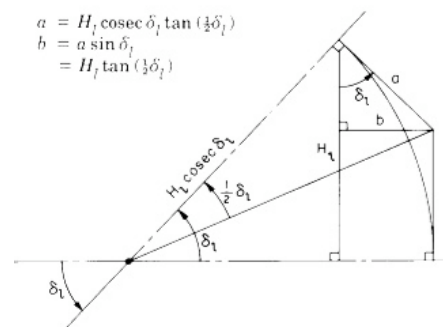
(b) Vented Krüger flap



$$c' = c + c_l - L_l - H_l \tan(\delta_l/2)$$

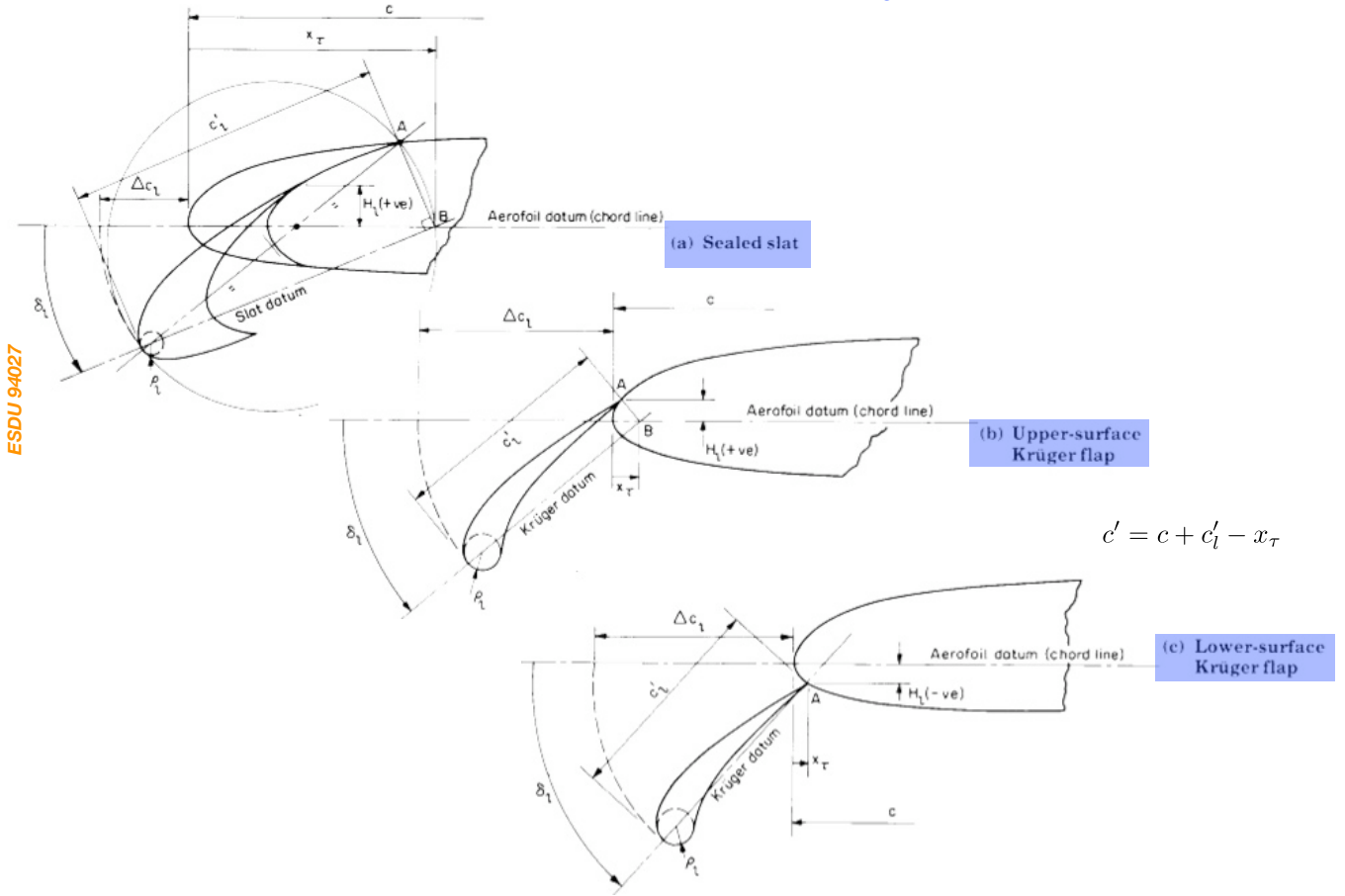
(c) Construction for c'
 [see Equations (4.4a) and (4.4b)]

$$\begin{aligned} a &= H_l \operatorname{cosec} \delta_l \tan(\tfrac{1}{2} \delta_l) \\ b &= a \sin \delta_l \\ &= H_l \tan(\tfrac{1}{2} \delta_l) \end{aligned}$$



$$c_l' = c_l - H_l / \sin \delta_l$$

ESDU LE device effects on C_{lmax} — 3



ESDU LE device effects on C_{lmax} — 4

3.1 Increment in Lift Coefficient at Zero Angle of Attack

The deployment of a leading-edge device gives a (usually small) loss in aerofoil lift at zero angle of attack, determined from

$$\Delta C'_{L0l} = [\Delta C'_{L0l}]_1 + [\Delta C'_{L0l}]_2 \quad (3.1)$$

The prime symbol (') indicates that the lift coefficient increment is based on the aerofoil extended chord c' .

In Equation (3.1) the first term is the main contribution obtained from the theory, and is given by

$$[\Delta C'_{L0l}]_1 = K_0 a_l \delta_l \quad (3.2)$$

where K_0 is an empirical correlation factor, which is dependent upon the type of leading-edge device, and a_l is the theoretical rate of change of lift coefficient with respect to the deflection δ_l , positive nose down, given by thin plate theory as

$$a_l = -2(\theta_l - \sin \theta_l) \quad (3.3)$$

$$\text{where } \theta_l = \cos^{-1}(1 - 2c_{el}/c') \quad (3.4)$$

$$\text{and } \sin \theta_l = [1 - (1 - 2c_{el}/c')^2]^{1/2}, \quad (3.5)$$

in which c_{el} is the effective chord of the leading-edge device.

Combination of Equations (3.2) to (3.5) gives, in conjunction with Equation (3.1),

$$\Delta C'_{L0l} = -2K_0 \delta_l \{ \cos^{-1}(1 - 2c_{el}/c') - [1 - (1 - 2c_{el}/c')^2]^{1/2} \} + [\Delta C'_{L0l}]_2, \quad (3.6)$$

in which $[\Delta C'_{L0l}]_2$ is a correction required only for slats and vented Krüger flaps.

To convert the lift coefficient based on extended chord to one based on basic aerofoil chord, the equation

$$\Delta C_{L0l} = (c'/c) \Delta C'_{L0l} \quad (3.7)$$

is used. The value of ΔC_{L0l} can be taken to be independent of Reynolds number.

ESDU LE device effects on C_{lmax} — 5

3.2 Increment in Maximum Lift Coefficient

The increment in maximum lift coefficient is given by

$$\Delta C'_{Lml} = K_e K_g K_l a_{ml} (\delta_l - \delta_0) \quad (3.8)$$

For given flow conditions the empirical correlation factors K_e , K_g and K_l are dependent only upon leading-edge device geometry. In this Item K_e , K_g and K_l have been determined for a datum Reynolds number of $R_c = 3.5 \times 10^6$ (see Section 5). The parameter a_{ml} is the theoretical rate of change of maximum lift coefficient with respect to δ_l , given by thin plate theory as

$$a_{ml} = 2 \sin \theta_l \quad (3.9)$$

in which $\sin \theta_l$ is given by Equation (3.5).

Equation (3.8) can be rewritten, using Equations (3.9) and (3.5), as

$$\Delta C'_{Lml} = 2 K_e K_g K_l (\delta_l - \delta_0) [1 - (1 - 2 c_{el}/c')^2]^{1/2}, \quad (3.10)$$

for the datum Reynolds number. The parameter δ_0 is the empirically-derived value of δ_l required to give $\Delta C'_{Lml} = 0$ for slats and vented Krüger flaps.

The magnitude of ΔC_{Lml} is influenced by Reynolds number. Analysis of data in Derivations 10 and 14 showed that if K_e , K_g and K_l were correlated at a datum Reynolds number, taken here as $R_c = 3.5 \times 10^6$, then all the Reynolds number dependence of ΔC_{Lml} could be allowed for through a factor, F_R , given by

$$F_R = 0.153 \log_{10} R_c, \quad (3.11)$$

which is unity at the datum.

Thus

$$\Delta C_{Lml} = F_R (c'/c) \Delta C'_{Lml}. \quad (3.12)$$

ESDU LE device effects on C_{lmax} — 6

4. DETERMINATION OF $\Delta C'_{L0l}$ AND $\Delta C'_{Lml}$ FOR A RANGE OF LEADING-EDGE HIGH-LIFT DEVICES

To determine values of $\Delta C'_{L0l}$ and $\Delta C'_{Lml}$, and thence to determine the associated values of ΔC_{L0l} and ΔC_{Lml} , for the various types of leading-edge device, Equations (3.6) and (3.10) are used in conjunction with Equations (3.7) and (3.12). The parameters involved in Equations (3.6) and (3.10) take different values according to the type of leading-edge device, so Table 4.1 is presented to show the source of the required geometry and definitions or locations whereby the relevant parameters can be determined.

TABLE 4.1 Source of geometry and relevant parameters required for evaluation of Equations (3.6) and (3.10) for various leading-edge devices

Leading-edge device	Geometry in Section	Parameter in Equation (3.6) or (3.10)							
		c_{el}	δ_l	K_0	$[\Delta C'_{L0l}]_2$	K_e	K_g	K_l	δ_0
Plain leading-edge flaps and drooped leading edges	4.1	c'_l	Sketch 4.1	$1/K_l$	0	1.0	Fig. 2a	Fig. 1a	0
Slats and vented Krüger* flaps	4.2	c_l	Sketch 4.2	1.35	0.030	Fig 3 for slats, 1.0 for vented Krügers	Fig. 2b	Fig. 1b	0.25
Krüger* flaps and sealed slats	4.3	c'_l	Sketch 4.3	1.8	0	1.0	Fig. 2a	Fig. 1c	0

* It is essential to refer to Section 4.3 for the determination of ΔC_{Lml} for Krüger flaps (vented or unvented) for details of a limitation on Krüger nose geometry.

In addition to the sketches, Sections 4.1 to 4.3 contain special comments concerning the geometry and its influence on $\Delta C'_{L0l}$ or $\Delta C'_{Lml}$ via the correlation parameters.

ESDU LE device effects on C_{lmax} — 7

ESDU 94027

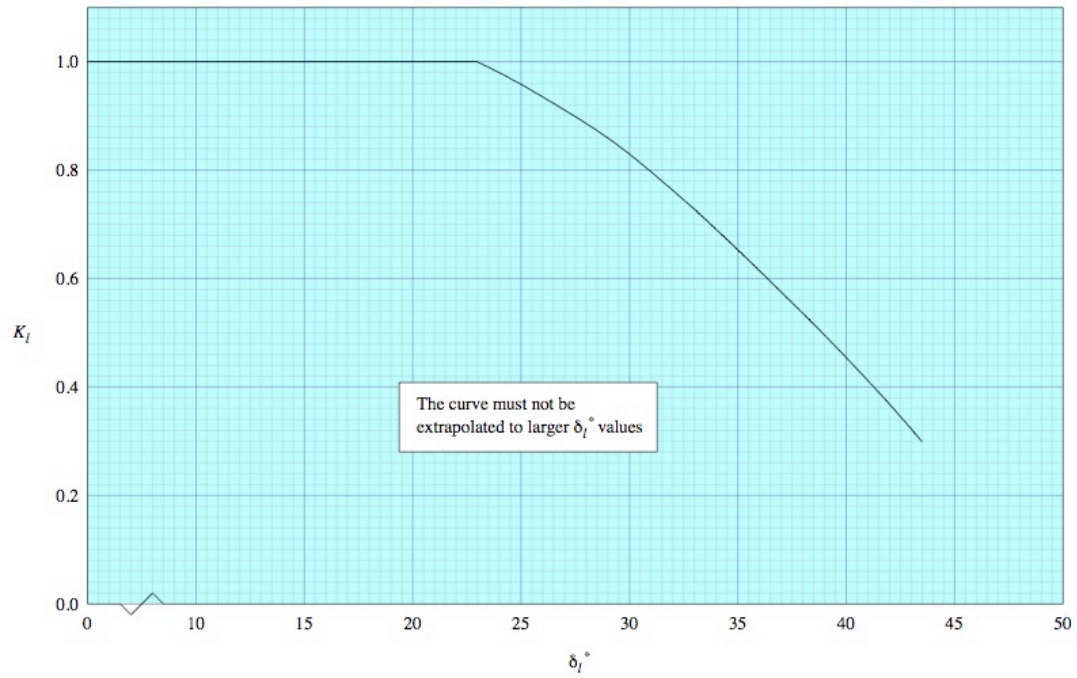


FIGURE 1a CORRELATION FACTOR K_l – Plain leading-edge flaps and drooped leading edges

ESDU LE device effects on C_{lmax} — 8

ESDU 94027

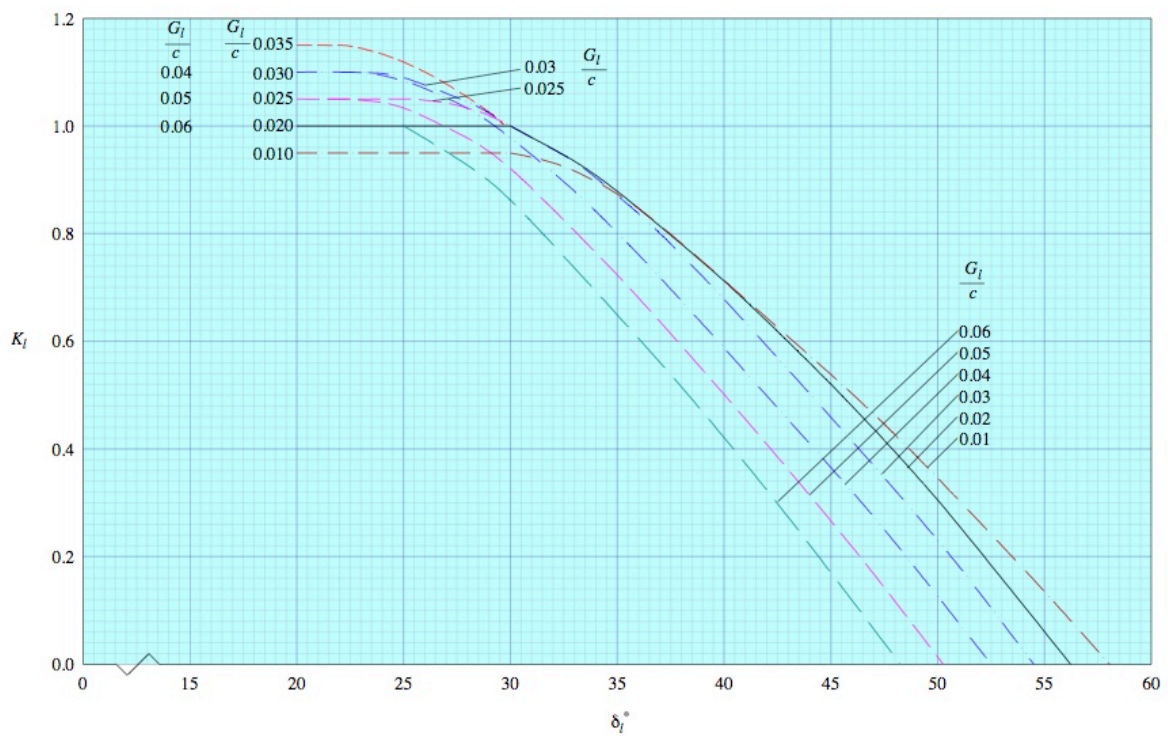


FIGURE 1b CORRELATION FACTOR K_l – Slats and vented Krüger flaps

ESDU LE device effects on C_{lmax} — 9

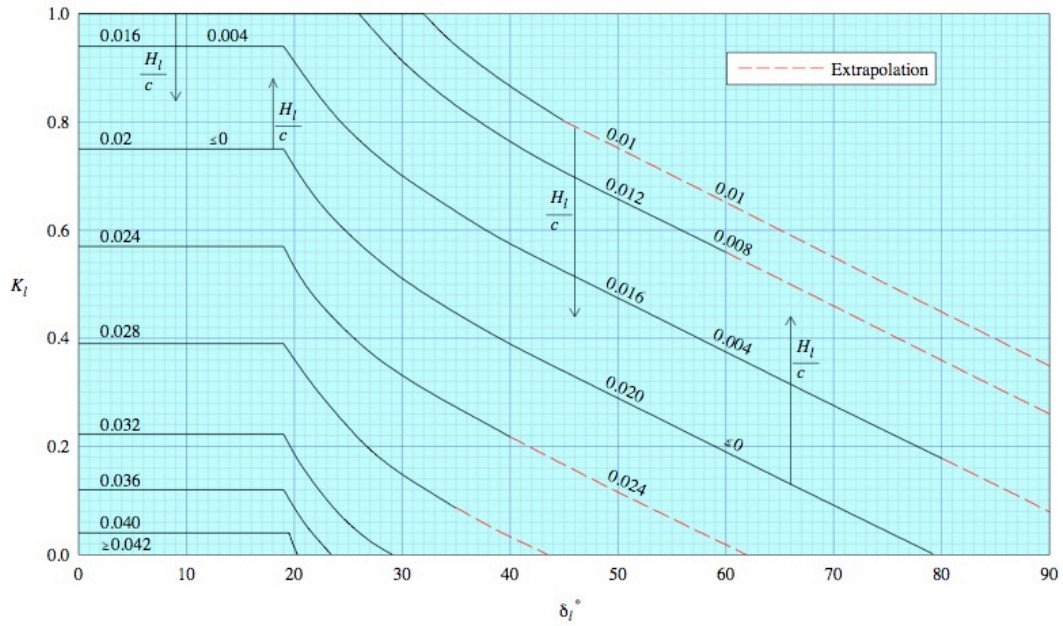


FIGURE 1c CORRELATION FACTOR K_l – Krüger flaps and sealed slats

ESDU LE device effects on C_{lmax} — 10

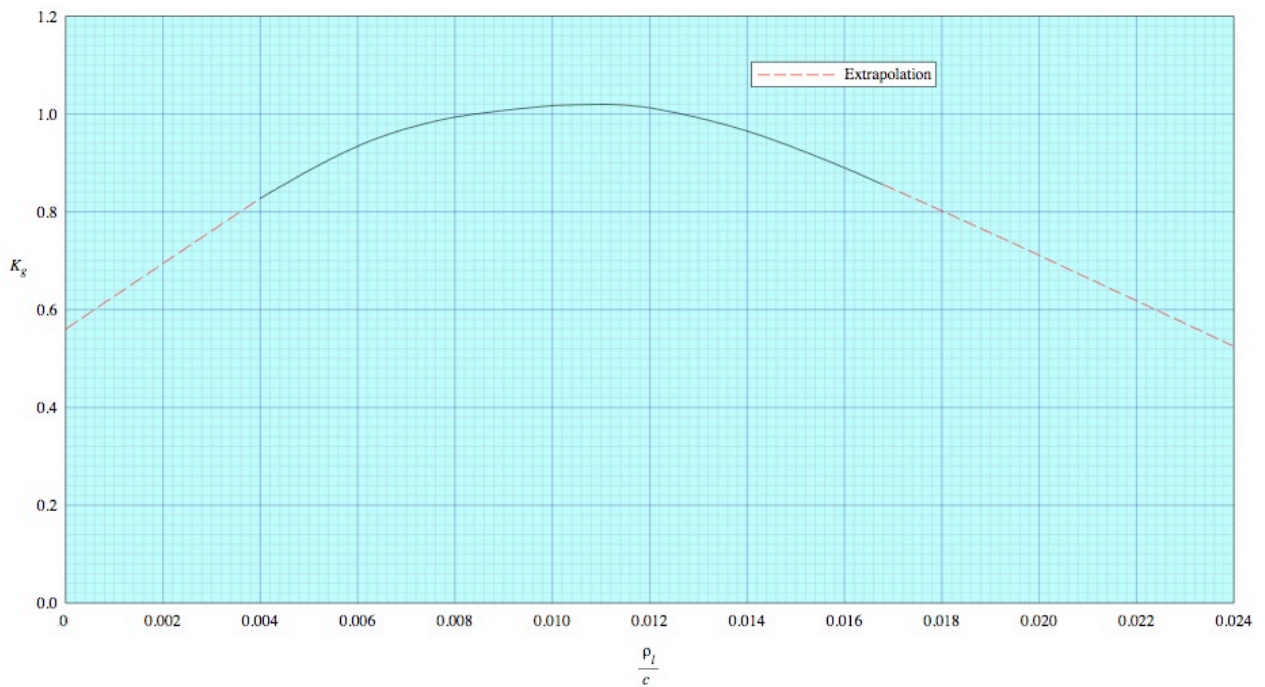


FIGURE 2a CORRELATION FACTOR K_g – Leading-edge flaps, drooped leading edges, Krüger flaps and sealed slats

ESDU LE device effects on C_{lmax} – 11

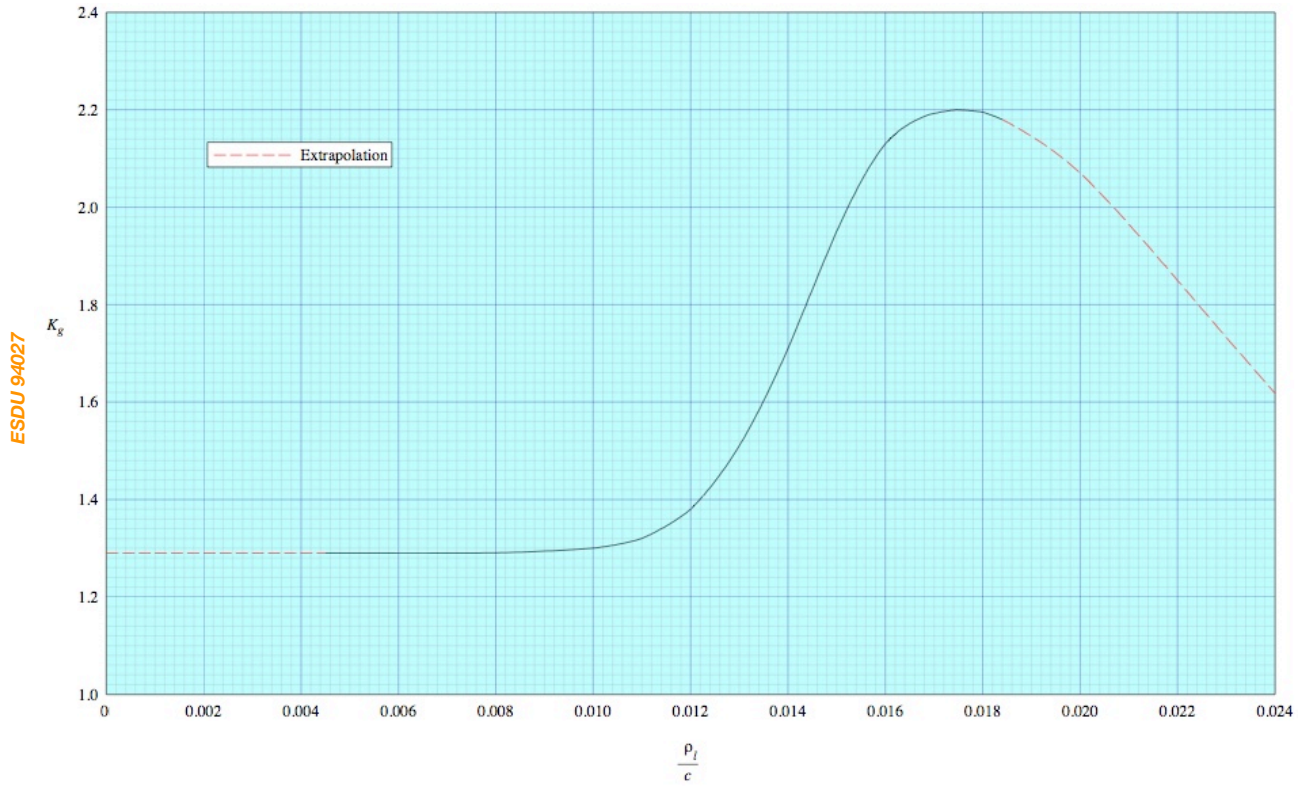


FIGURE 2b CORRELATION FACTOR K_g – Slats and vented Krüger flaps

ESDU LE device effects on C_{lmax} – 12

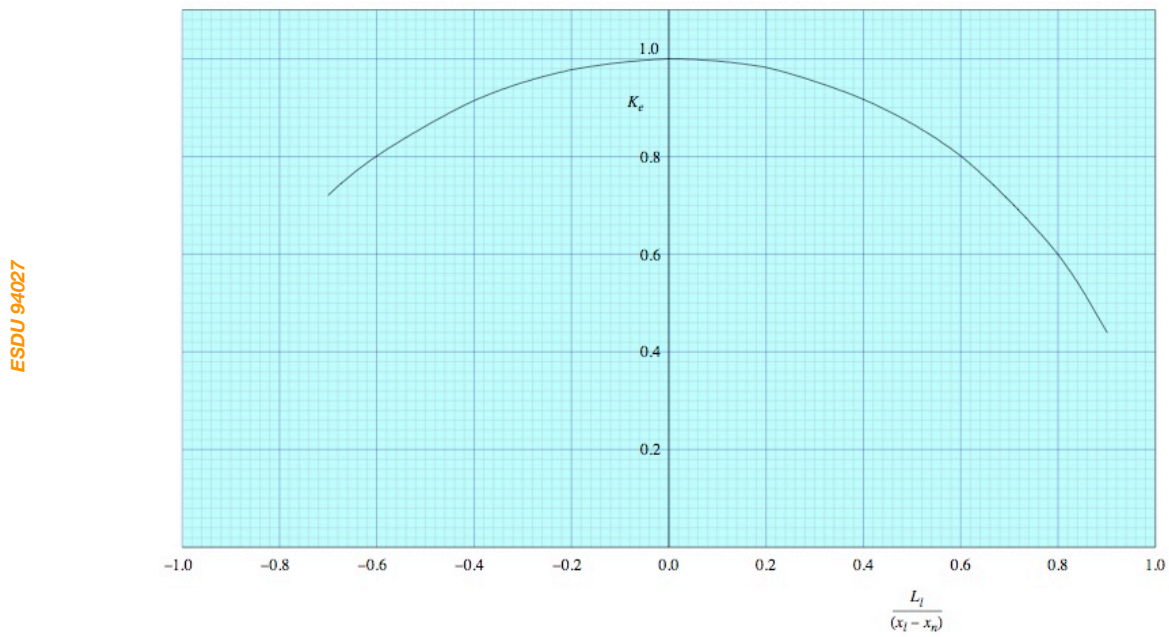


FIGURE 3 CORRELATION FACTOR K_e

ESDU LE device effects on C_{lmax} — 13

5. APPLICABILITY AND ACCURACY

5.1 Applicability

The methods given in this Item for estimating the increments in aerofoil lift coefficient at zero angle of attack and in maximum lift coefficient due to the deployment of leading-edge high-lift devices are applicable to a wide range of such devices. Table 5.1 gives the ranges of parameters covered by measured data, obtained from Derivations 1 to 9 and 12, for which the various correlation factors used in developing the methods have been obtained.

TABLE 5.1 Parameter ranges for test data used in methods of Section 4

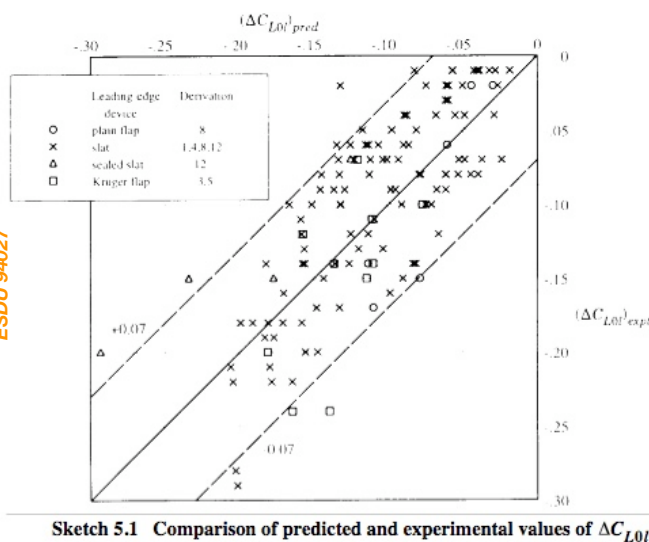
Parameter	Plain leading-edge flaps and drooped leading edges	Slats and vented Krüger flaps	Krüger flaps and sealed slats
t/c	0.06 to 0.10	0.09 to 0.15	0.09 to 0.15
ρ_l/c	0.004 to 0.0069	0.005 to 0.0158	0.0055 to 0.015
ρ_l/t	0.067 to 0.0687	0.055 to 0.132	0.061 to 0.10
x_n/c	Not applicable	0.0185 to 0.05	Not applicable
c_{el}/c	0.15	0.125 to 0.218	0.097 to 0.306
δ_l° (undeflected)	Not applicable	13° to 27°	Not applicable
δ_l°	0 to 45°	12° to 50°	12° to 92°
L_l/c	Not applicable	-0.028 to 0.125	Not applicable
H_l/c	Not applicable	-0.020 to 0.088	-0.0204 to 0.045
G_l/c	Not applicable	0.01 to 0.06	Not applicable
x_τ/c	Not applicable	Not applicable	0.02 to 0.25
$R_c \times 10^{-6}$	4.5 to 6.0	0.60 to 6.0	0.8 to 6.0
M	0.15 to 0.17	0.10 to 0.17	0.11 to 0.17

The methods are based on the theoretical effects derived from simple thin hinged-plate theory with empirical corrections for the effects of practical leading-edge device geometry. The leading-edge device requiring the largest number of such corrections is the slat (including the vented Krüger flap). That is not surprising since it is the device farthest removed from a simple hinged plate in terms of the physical processes involved in its operation. The slot is very influential in its own right; in the extreme case a slat can provide a change in maximum lift simply by translation, with no rotation, to open up a slot.

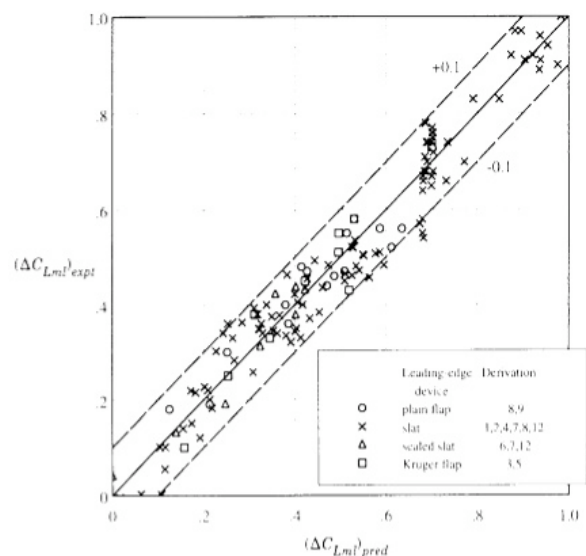
ESDU LE device effects on C_{lmax} — 14

ESDU 94027

ESDU 94027



Accuracy approx. $\pm 7\%$



Accuracy approx. $\pm 10\%$

Accuracy approx. $\pm 10\%$

ESDU TE device (single-slotted flap) effects on C_{lmax} — 1

3. LIFT COEFFICIENT INCREMENTS ΔC_{L0} AND ΔC_{Lm}

The increments in the lift coefficient at zero angle of attack, ΔC_{L0} , and at maximum lift, ΔC_{Lm} , due to the deployment of a leading-edge high-lift device and a trailing-edge flap on an aerofoil are given by the sum of the individual increments, *i.e.*

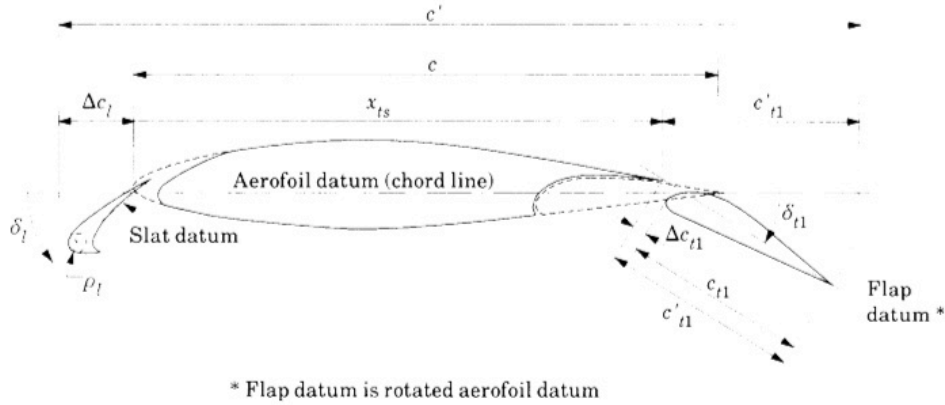
$$\Delta C_{L0} = \Delta C_{L0l} + \Delta C_{L0t} \quad (3.1)$$

$$\text{and} \quad \Delta C_{Lm} = \Delta C_{Lml} + \Delta C_{Lmt} \quad (3.2)$$

$$\Delta C_{L0t} = \frac{c'}{c} \Delta C'_{L0t} \quad (3.3)$$

$$\text{and} \quad \Delta C_{Lmt} = F_R \frac{c'}{c} \Delta C'_{Lmt} \quad (3.4)$$

$$\text{where} \quad F_R = 0.153 \log_{10} R_c \quad (3.5)$$



Sketch 4.1 Single-slotted trailing-edge flap with typical leading-edge high-lift device (slat)

ESDU TE device (single-slotted flap) effects on C_{lmax} — 2

4.1 Increment in Lift Coefficient at Zero Angle of Attack

The increment in lift coefficient at zero angle of attack due to the deployment of a single-slotted trailing-edge flap is given by

$$\Delta C'_{L0t} = J_{t1} \Delta C'_{L1} (a_1)_0 / 2\pi \quad (4.1)$$

In this equation J_{t1} is an empirical correlation (or efficiency) factor which is a function of δ_{t1} and is given by

$$J_{t1} = 1.17 [\sin(3.83\delta_{t1}^\circ)]^{1/2} \quad \text{for } 0 \leq \delta_{t1}^\circ \leq 23.5^\circ \quad (4.2)$$

$$\text{and} \quad J_{t1} = 1.17 \quad \text{for } \delta_{t1}^\circ > 23.5^\circ, \quad (4.3)$$

which are plotted in Figure 1.

The flap deflection, δ_{t1} , is seen from Sketch 4.1 to be the angle through which the flap datum* is rotated relative to the stowed flap situation. Thus, for a single-slotted flap δ_{t1} is the angle through which the aerofoil datum is rotated.

The lift coefficient increment, $\Delta C'_{L1}$, associated with the deployment of a single-slotted flap on an aerofoil having a lift-curve slope of 2π , is based on Item No. Flaps 01.01.08 (Derivation 19) and is given in Figure 2 as a function of δ_{t1}° and c'_{t1}/c' . The parameter $\Delta C'_{L1}$, which is based on test data, replaces the value derived from thin plate theory used for plain flaps in Item No. 94028. This was necessary because slot effects are not represented in the simple theory.

ESDU TE device (single-slotted flap) effects on C_{lmax} — 3

4.2 Increment in Maximum Lift Coefficient

In the development of the method for predicting the increment in maximum lift coefficient it was found necessary to adapt further the thin hinged plate theoretical model to cater for slotted flaps, especially those involving large chord extensions. *i.e.* Fowler flaps. With such flaps it is possible to obtain significant increments in maximum lift (with a low drag penalty) by deployment with zero deflection. The increment in maximum lift is then very largely due to chord extension and is related to the basic aerofoil maximum lift. The increment in maximum lift coefficient then consists of two components, one, $(\Delta C'_{Lmt})_0$, independent of flap deflection and the other, $(\Delta C'_{Lmt})_1$, due to the deflection. Thus

$$\Delta C'_{Lmt} = (\Delta C'_{Lmt})_0 + (\Delta C'_{Lmt})_1, \quad (4.6)$$

where

$$(\Delta C'_{Lmt})_0 = (1 - c'/c)(C_{LmB})_d \quad (4.7)$$

and

$$(\Delta C'_{Lmt})_1 = K_T K_{t1} J_{t1} \Delta C'_{L1} - (1 - c'/c) \sin \delta_{t1} (C_{LmB})_d, \quad (4.8)$$

so that

$$\Delta C'_{Lmt} = (1 - c'/c)(1 - \sin \delta_{t1})(C_{LmB})_d + K_T K_{t1} J_{t1} \Delta C'_{L1}. \quad (4.9)$$

In Equation (4.9) $(C_{LmB})_d$ is the maximum lift coefficient for the basic aerofoil at the datum Reynolds number $R_c = 3.5 \times 10^6$, obtained from Item No. 84026 (Derivation 25).

The extended chord, c' , is given by Equations (4.4) and (4.5), J_{t1} is obtained either from Figure 1 or from Equation (4.2) or (4.3) and $\Delta C'_{L1}$ is obtained from Figure 2.

The correlation factor K_T , given in Figure 3, allows for the effect of basic aerofoil geometry via $z_{u1.25}/c$, the dimensionless upper-surface ordinate at 0.0125c, and x_{um}/c , the dimensionless chordwise location of the maximum upper-surface ordinate. Values of $z_{u1.25}/c$ for a range of NACA sections are given in Item No. 66034 (Reference 28). The correlation factor K_{t1} is given as a function of δ_{t1}° in Figure 4.

Finally, with the value of $\Delta C'_{Lmt}$ obtained from Equation (4.9), ΔC_{Lmt} is evaluated from Equation (3.4) with F_R given by Equation (3.5).

ESDU TE device (single-slotted flap) effects on C_{lmax} — 4

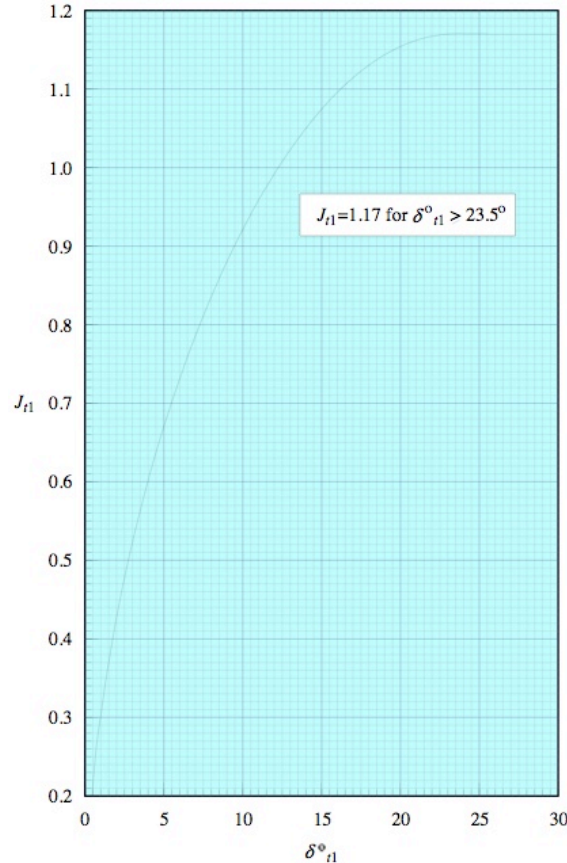


FIGURE 1

ESDU TE device (single-slotted flap) effects on C_{lmax} — 5

ESDU 94030

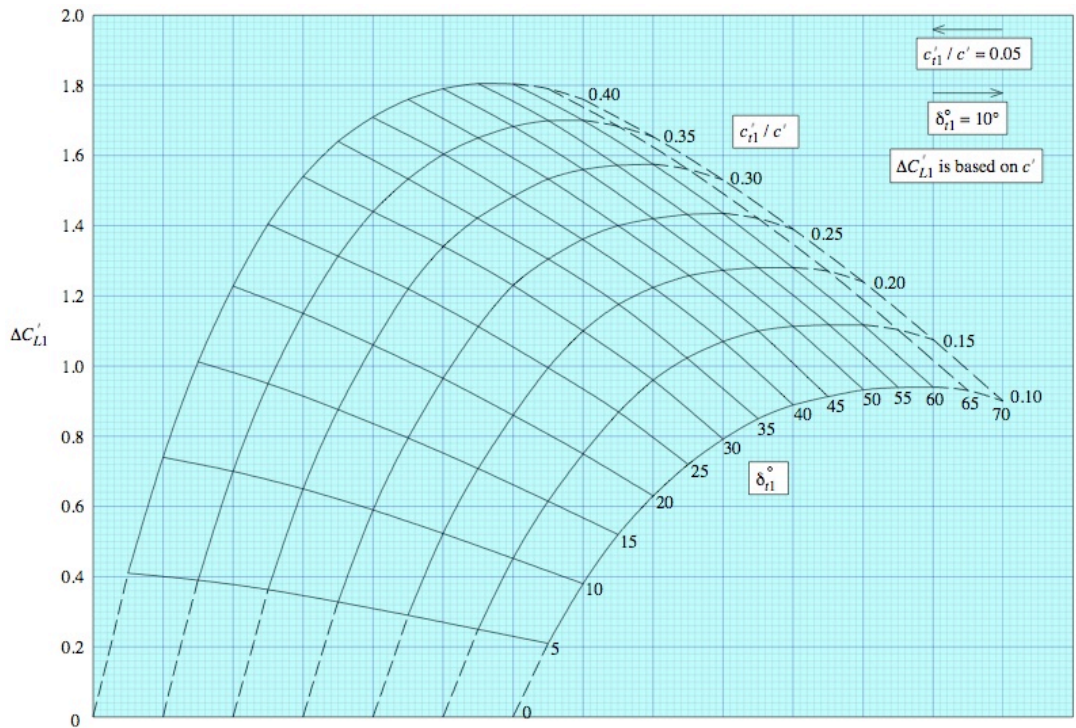


FIGURE 2

ESDU TE device (single-slotted flap) effects on C_{lmax} — 6

ESDU 94030

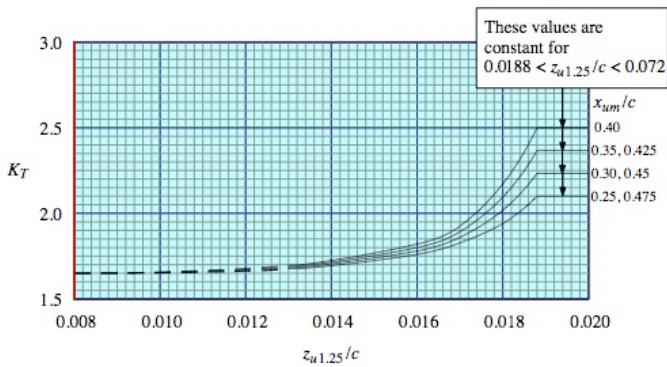


FIGURE 3

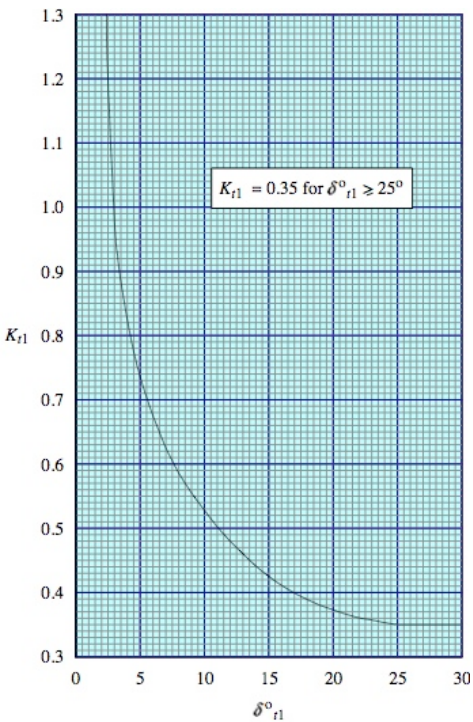


FIGURE 4

ESDU TE device (single-slotted flap) effects on C_{lmax} — 7

ESDU 94030

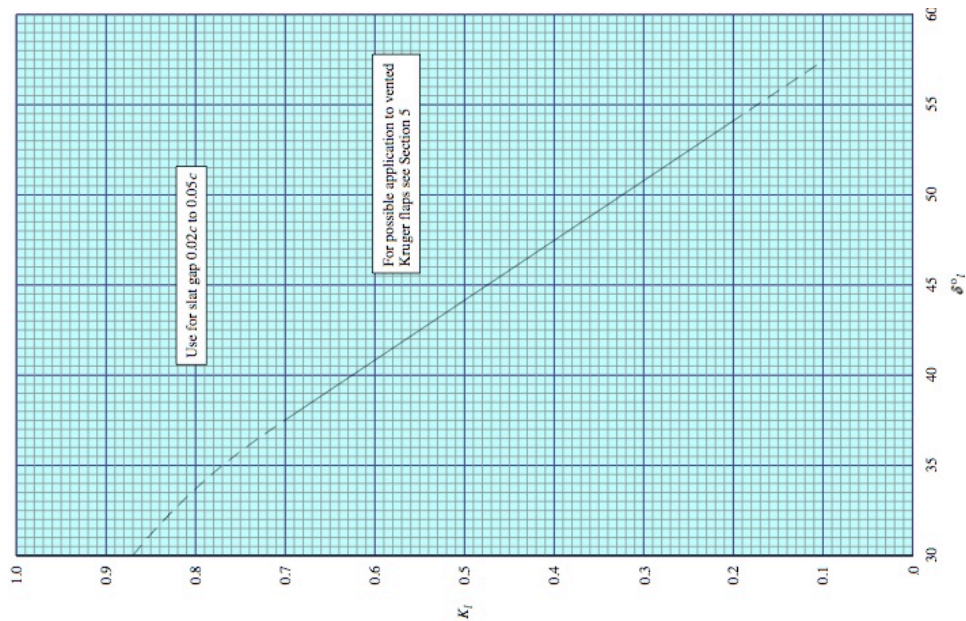


FIGURE 5 CORRELATION FACTOR K_l FOR SLATS IN PRESENCE OF TRAILING-EDGE SLOTTED FLAPS

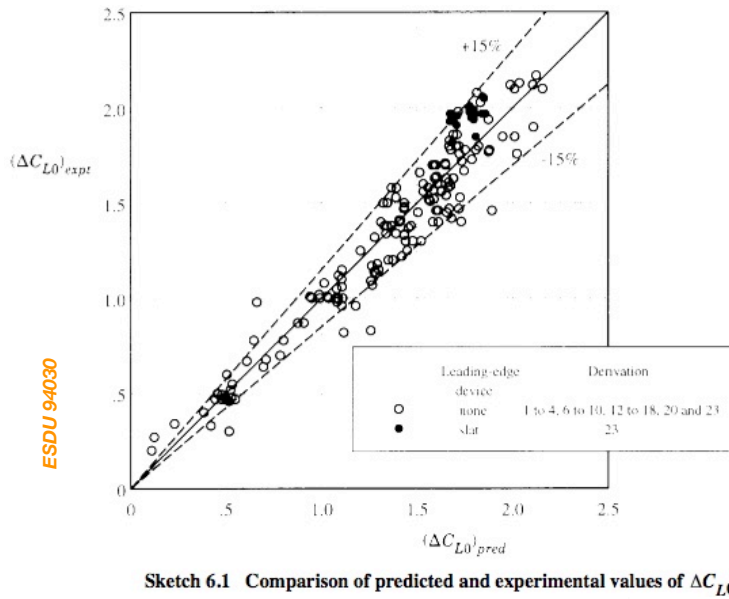
ESDU TE device (single-slotted flap) effects on C_{lmax} — 8

ESDU 94030

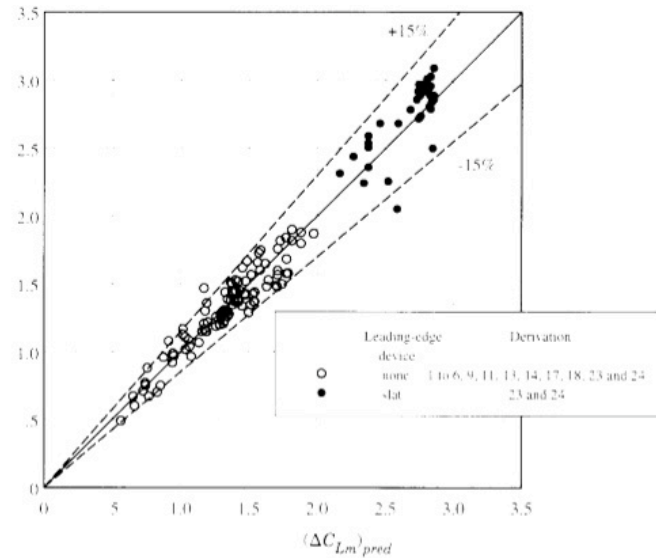
TABLE 6.1 Parameter ranges for test data for single-slotted trailing-edge flaps used in methods of Section 4

Parameter	Ranges
t/c	0.10 to 0.30
ρ_l/c	0.007 to 0.099
$z_{u1.25}/c$	0.013 to 0.072
x_{um}/c	0.25 to 0.45
x_{ts}/c	0.715 to 1.000
c_{t1}^l/c	0.15 to 0.40
δ_{r1}^o	0 to 60°
c'/c (no slat)	1.02 to 1.42
c'/c (with slat)	1.27 to 1.39
$R_c \times 10^{-6}$	1.0 to 9.0
M	0.12 to 0.24

ESDU TE device (single-slotted flap) effects on $C_{l_{max}}$ — 9

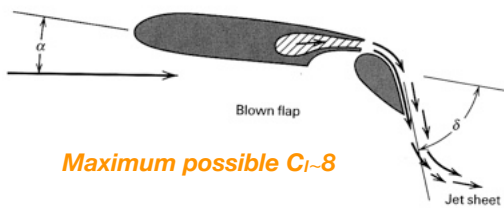


Accuracy approx. $\pm 15\%$

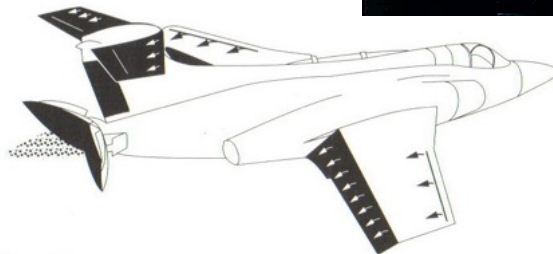


BL blowing/suction to raise $C_{l_{max}}$

When wing loadings are very high, engine-powered BL suction or (more usually) blowing can maintain attached flow and significantly increase $C_{l_{max}}$ at the expense of added complexity, weight, and reduced reliability.



BL blowing may occur near LE without any movable airfoil element, as well as over flaps (e.g. Buccaneer).

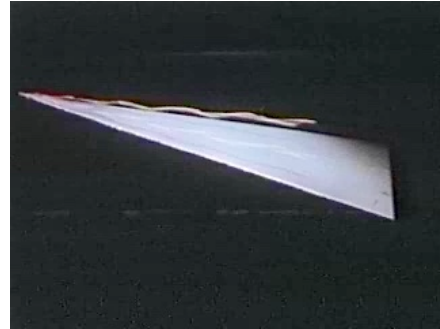


The TSR-2 employed blown flaps. Take-off distance was reduced from 2800m to 750m.

The F104 employed blown flaps to reduce landing speeds to tolerable values.



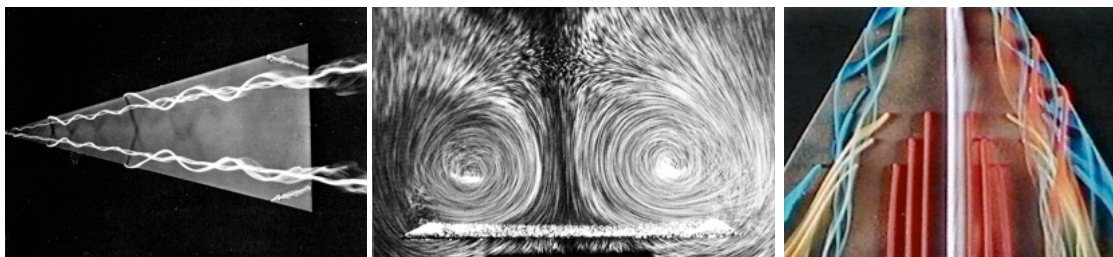
High- α aerodynamics for swept wings



1. On highly-swept wings, flow initially detaches from the LE as α increases, and may roll up into vortices that produce substantial lift (aka vortex lift).
2. In this case, stall is not closely linked to the onset of flow separation and lift may be further increased by raising α still higher.
3. The penalty is that drag is also large. However, the L/D ratio may be acceptable for the flight phase considered.
4. Typically, high- α effects are mainly relevant to sub/transonic flight. Supersonic aircraft may however (and often do) exploit this effect to lift for takeoff, landing, or (subsonic) manoeuvring.
5. If the wing is not highly-swept, chines or LE extensions (LEX) near the wing root can be used to induce vortex flows.

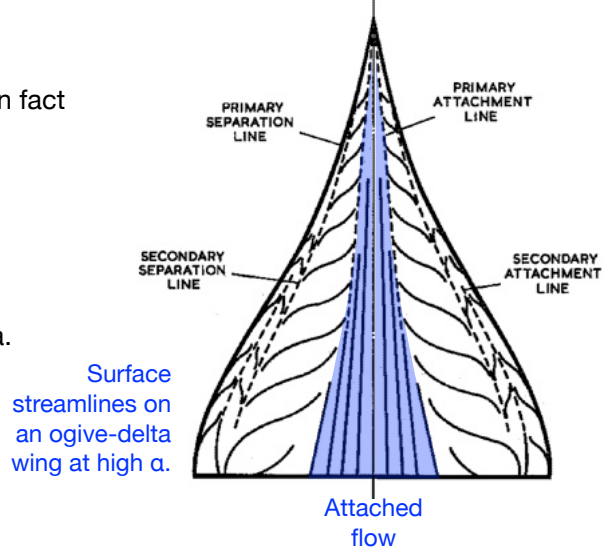
High- α aerodynamics for delta wings — 1

On delta wings, which are typically highly-swept, a reasonable approximation for high- α lift and drag is obtained by assuming the lift is provided by a combination of 'potential' and 'vortex' lift.



At first this might not seem a very good idea but in fact there typically is a region of flow between the LE vortices that is non-swirling and much like the predictions of slender-wing potential flow.

First we examine the slender-wing potential flow theory of Jones and then the cross-flow drag idea. A modified sum of these (Polhamus' theory) does a reasonable job.

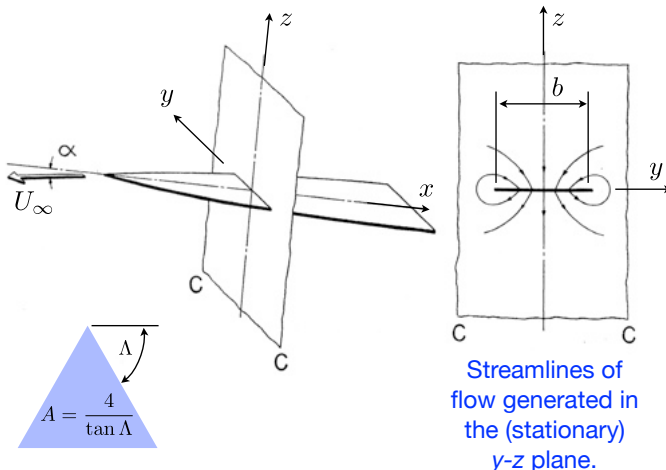


Jones' theory for slender wings of low aspect ratio — 1

RT Jones in effect made the dual of Prandtl's assumptions for slender wings of high aspect ratio:

1. The flow around every cross-section perpendicular to the flight direction can be approximated by the two-dimensional flow around the same section, superimposed on the original uniform stream.
2. This makes it possible to determine the lift distribution along the *chord* just as the Prandtl theory gives the lift distribution along the *span*.
3. The lift at any point is only influenced by the flow ahead of the point considered and is independent of the flow conditions downstream, whereas in Prandtl's case of large-aspect-ratio wings, the local lift depends largely on the influence of the free vortices downstream.

Consider a delta wing flying through a stationary body of fluid, with AoA α :



The flow generated in the y-z plane is assumed to be the potential flow created by a flat plate of width b moving downwards at speed $U_\infty \sin \alpha$.

The increment in velocity potential between the two sides of the plate is given analytically by

$$\Delta\phi = U_\infty \sin \alpha b \sqrt{1 - \left(\frac{y}{b/2}\right)^2}$$

However, this 2D flow, if steady, will generate no force, because the flow is potential.

Jones' theory for slender wings of low aspect ratio — 2

The force is generated because in a fixed reference frame, the flow is unsteady owing to the passage of the wing. We can then use the unsteady Bernoulli equation (written in potential form)

$$\frac{\partial\phi}{\partial t} + \frac{p}{\rho} + \frac{1}{2}(\nabla\phi)^2 + gz = \text{const.}$$

to compute the lift force per unit length as

$$\begin{aligned} \frac{\partial L}{\partial x} &= \rho \frac{\partial}{\partial t} \int_{-b/2}^{b/2} \Delta\phi dy = \rho U_\infty \sin \alpha \frac{\partial}{\partial t} \int_{-b/2}^{b/2} b \sqrt{1 - \left(\frac{y}{b/2}\right)^2} dy \\ &= \rho U_\infty \sin \alpha \frac{\pi}{4} \frac{\partial b^2(x)}{\partial t} \end{aligned}$$

Use the chain rule

$$\begin{aligned} \frac{dL}{dx} &= \rho U_\infty \sin \alpha \frac{\pi}{4} \frac{db^2(x)}{dx} \frac{dx}{dt} \\ &= \frac{1}{2} \rho U_\infty^2 \pi \sin \alpha b(x) \frac{db(x)}{dx} \end{aligned}$$

Note there is no lift if $db/dx = 0$.

Now for a plain delta, $db/dx = \text{const}$ and we end up with

$$L = \frac{1}{2} \rho U_\infty^2 \frac{\pi}{2} \sin \alpha b_{\text{max}}$$

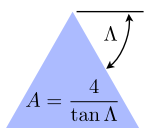
$$C_L = \frac{\pi}{2} A \sin \alpha$$

for lift, and

$$D_i = \frac{1}{2} L \sin \alpha$$

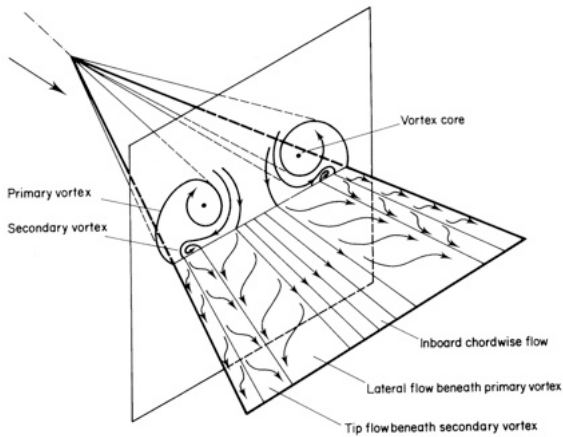
$$C_{Di} = \frac{C_L^2}{\pi A}$$

for induced drag.



Cross-flow drag analogy for detached component of vortex lift

Consider the normal force produced by the wing-normal component of flow, $U_\infty \sin \alpha$.



The wing is sharp-edged and this normal component of flow separates, giving rise to a wing-normal force with local drag coefficient, C_{DP} .

The force per unit length in the normal direction is:

$$\frac{1}{2} \rho U_\infty^2 \sin^2 \alpha b(x) C_{DP}$$

The lift force per unit length is the vertical component:

$$\frac{1}{2} \rho U_\infty^2 \sin^2 \alpha \cos \alpha b(x) C_{DP}$$

Total vortex lift force $L = \frac{1}{2} \rho U_\infty^2 \sin^2 \alpha \cos \alpha b(x) C_{DP} \int_0^c b(x) dx, \quad C_L = C_{DP} \sin^2 \alpha \cos \alpha$

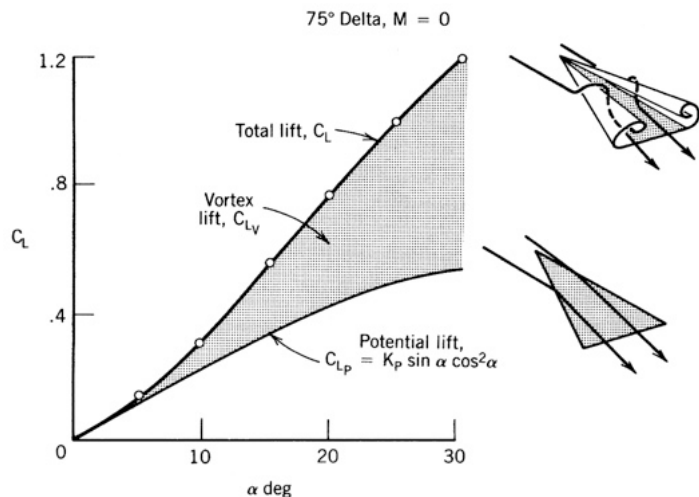
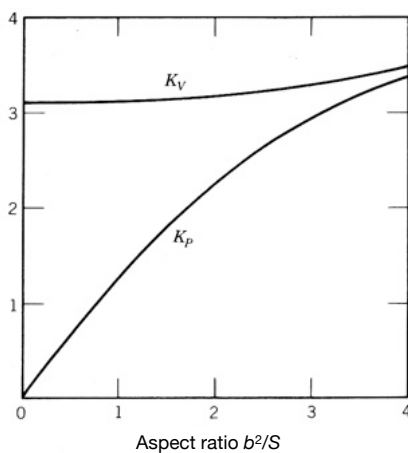
Polhamus' theory — 1

Using a leading-edge suction analogy to compute the separated flow/vortex lift component, and a potential-flow model for the remaining lift Polhamus (1966) derived

$$C_L = K_p \sin \alpha \cos^2 \alpha + K_v \cos \alpha \sin^2 \alpha, \quad C_D = C_L \tan \alpha$$

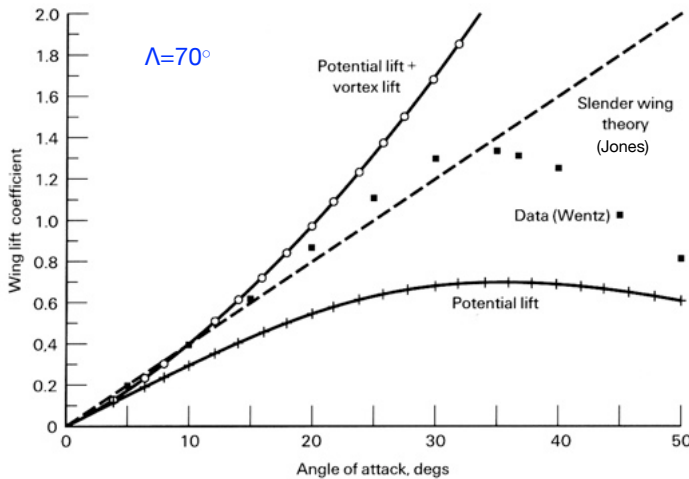
where K_p and K_v are respectively potential and vortex lift coefficients.

As $\alpha \rightarrow 0$, $C_L \rightarrow K_p \alpha$, so $K_p = \partial C_{LP} / \partial \alpha$.



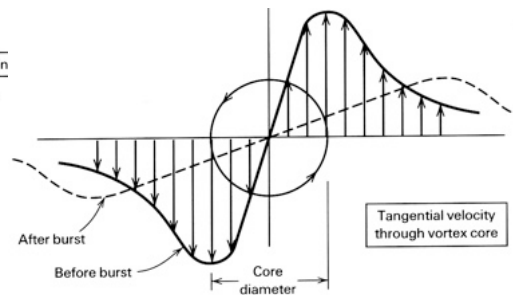
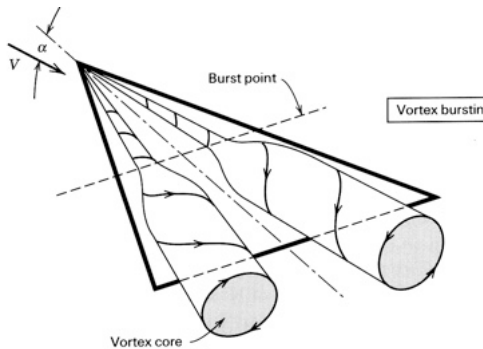
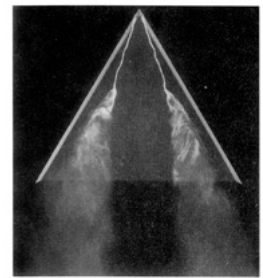
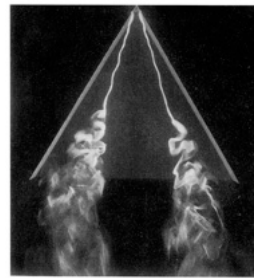
The model is found to do a reasonable job in subsonic flows provided α is not extreme.

Polhamus' theory — 2



(Reasonable agreement with Jones' theory at low α in this case 'is fortuitous'.)

Reduction in lift at high α is associated with onset of 'vortex bursting'.

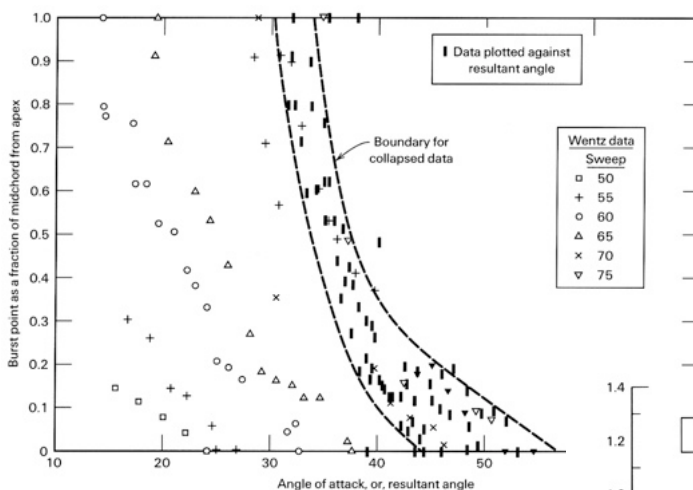


Vortex bursting tends to occur when the swirl strength as measured by $\tan^{-1}(V_\theta/V_x)$ is large.

The intense low pressure of the vortex cores, and hence much of the vortex lift, is lost.

Polhamus' theory — 3

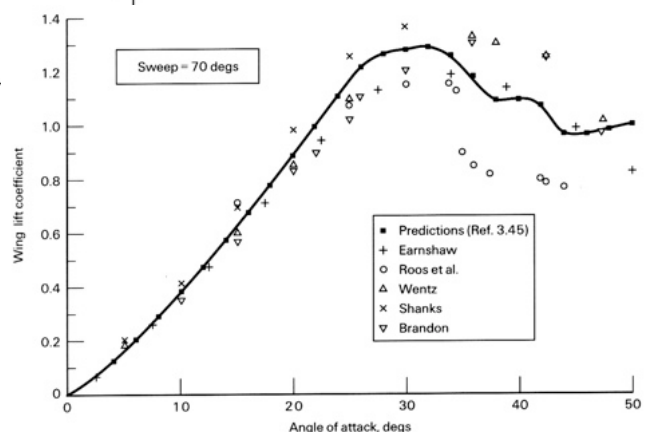
Since the circulation of the vortex increases downstream, the core will tend to burst with increasing x . Or α . Bursting can occur downstream of TE but this has no effect on a delta-winged aircraft.



Burst point data for different sweep and α collapse reasonably well with the 'resultant angle'

$$\beta = \cos^{-1}(\sin \Lambda \cos \alpha)$$

Quasi-empirical corrections then give an overall reasonable prediction of C_L .



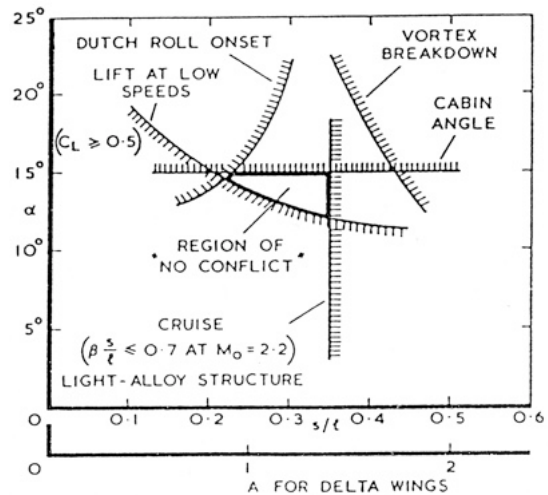
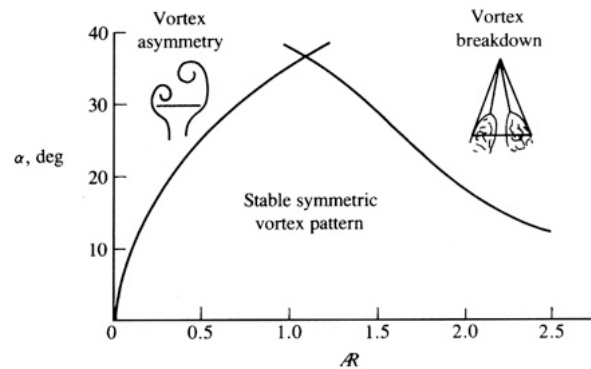
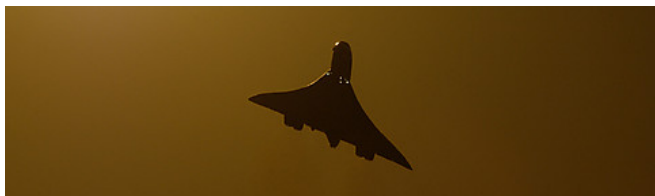
Delta wing design constraints

Besides vortex bursting, the LEVs shed from very slender/low A wings can interact, sometimes in an oscillatory fashion.

This supplies another design constraint.

Other constraints can be provided by the need to sweep the LE behind the Mach cone, or practical limits on cabin floor/cockpit α .

Overall, there is typically some window of feasibility.



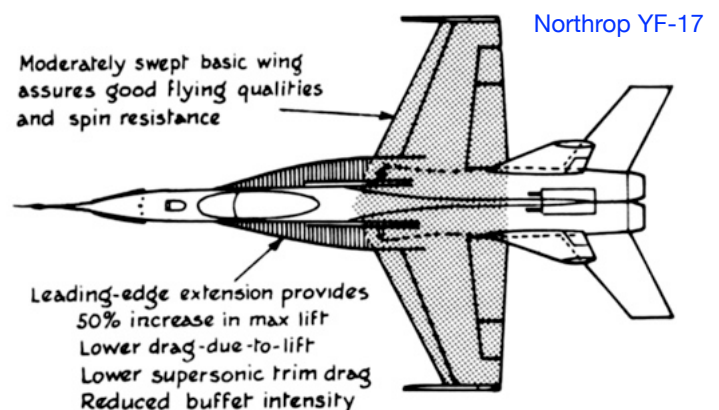
High- α aerodynamics with LE extensions (LEX) — 1

The impact of Concorde's successful exploitation of vortex lift boosted associated R&D for military application.



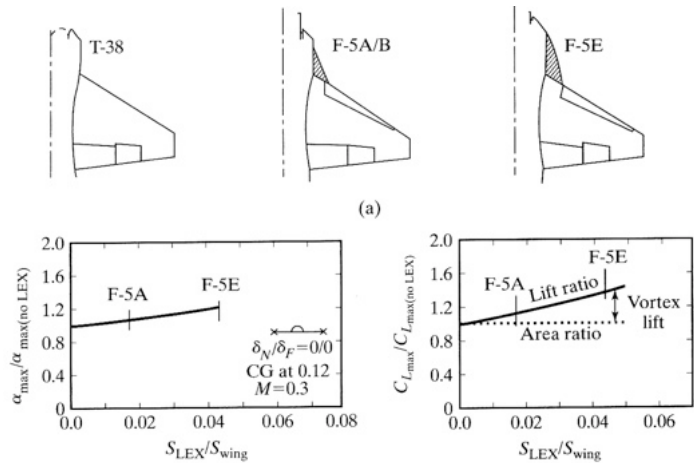
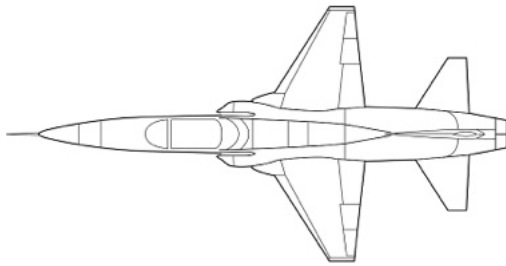
Meanwhile, some early adopters had already ceased production...

LEX provide little effect (other than aiding favourable axial area distribution for transonic regime) until high- α flows are encountered.

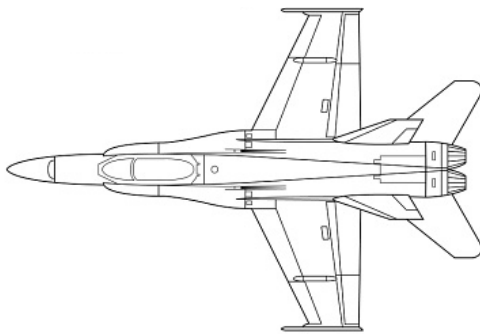


High- α aerodynamics with LEX — 2

Northrop's development of the F-5 family of wing designs showed a steady increase in high- α lift for small increments in area.



This led to the YF-17, then the F-18 series, both with comparatively larger LEX (approx 10% S).

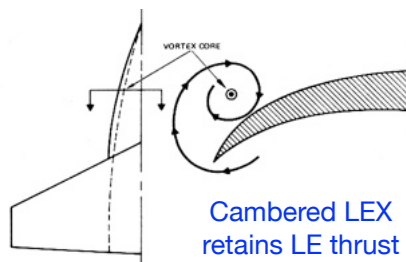
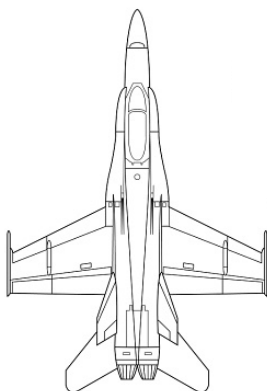


Note that the wing is designed with a supersonic LE, so is comparatively thin and sharp. To achieve best turning performance, both LE and TE manoeuvre flaps are also employed.

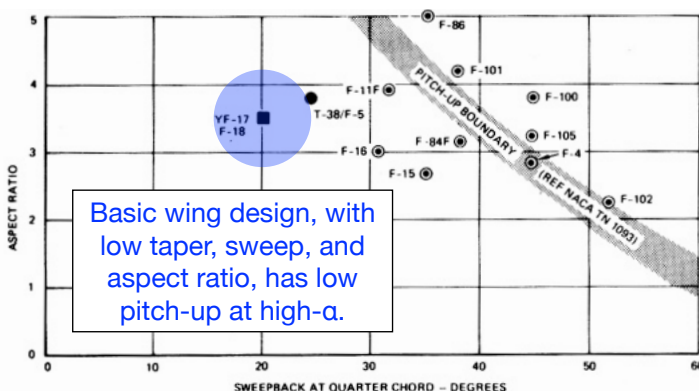
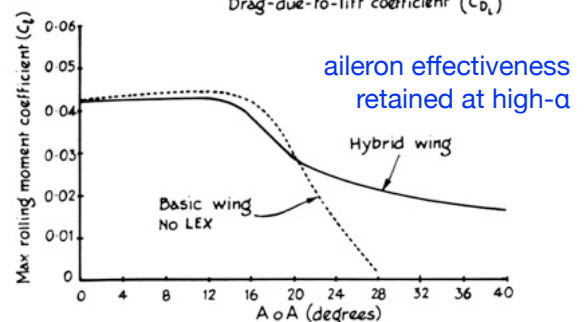
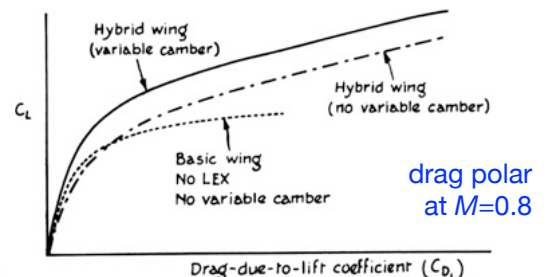
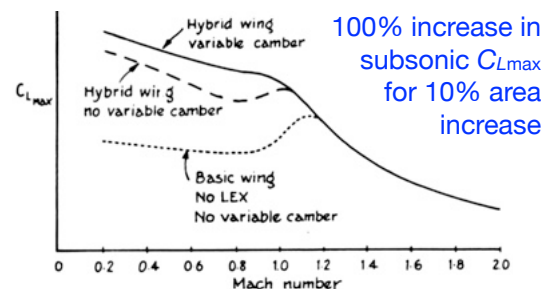
At higher wing loading than the F-15, comparable sustained turn rates are achieved, and the aircraft remains controllable at $\alpha \approx 45^\circ$ (or better).

High- α aerodynamics with LEX — 3

F-18 series performance characteristics

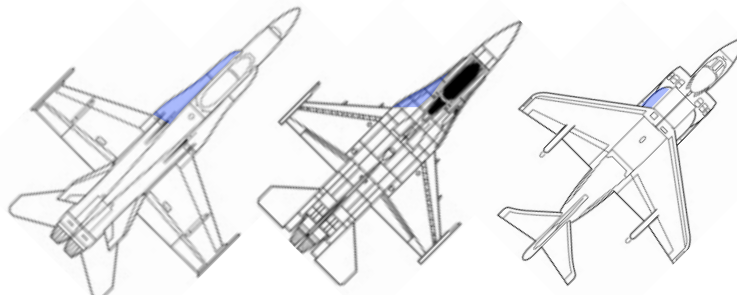


Cambered LEX retains LE thrust at high- α



High- α aerodynamics with LEX — 4

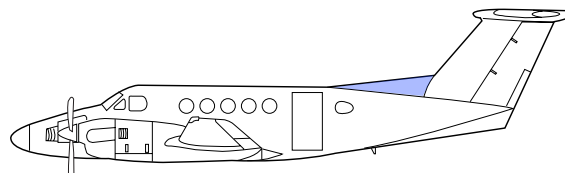
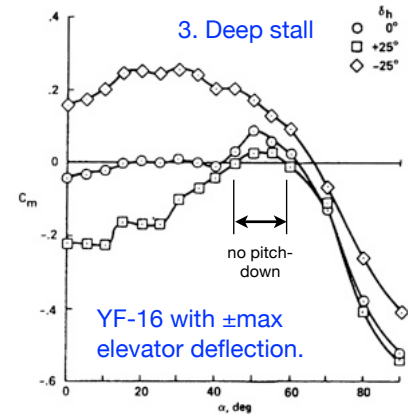
Related approaches have since been adopted on a variety of combat aircraft.



1. Vortex breakdown

2. Yaw departure

However, there have been some significant difficulties associated with heavy reliance on vortex lift:



Note that extended dorsal fins can be considered as fin LEX, adopted for good high- β characteristics.

Aerodynamic crutches — 1

Aerodynamic 'crutches' are add-on palliatives used to cure some undesirable aerodynamic characteristic, typically flow separation in an off-design situation. Very often they are seen on swept-wing aircraft.

Almost invariably, they rely on creating streamwise vortices on the wing upper surface.

The successful, routine use of wings swept back at 30 to 45 degrees is a source of wonder to stability and control engineers who were active in the 1940s. Then, a wing that was tapered by sweeping back the leading edge while keeping a straight or slightly swept trailing edge, giving no more than 5 degrees sweepback, was deplored. One could expect early wing tip stall with increasing angle of attack, wing drop, and roll-damping reversal.

(Abzug & Larrabee)

Aerodynamic palliatives ... are in a sense the vacuum cleaners of the aerodynamicist.

(Stinton)

... there is no such thing as a clean swept wing.

(Shevell)



Fences



Saw-tooth



Fence



Vortex generators

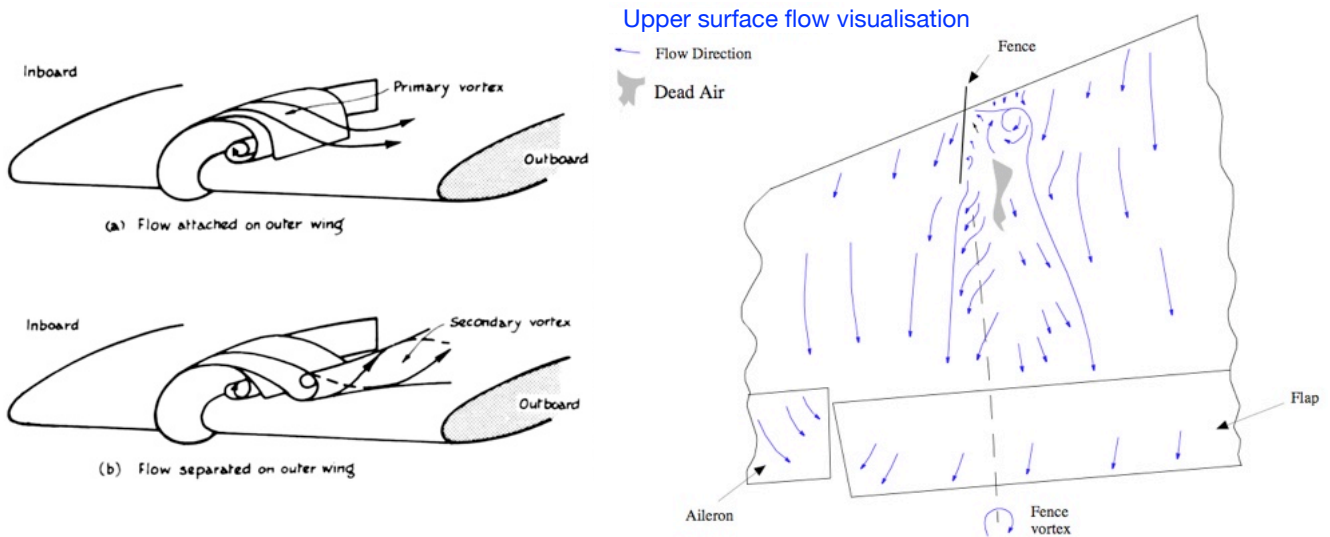


Notch

Aerodynamic crutches — 2

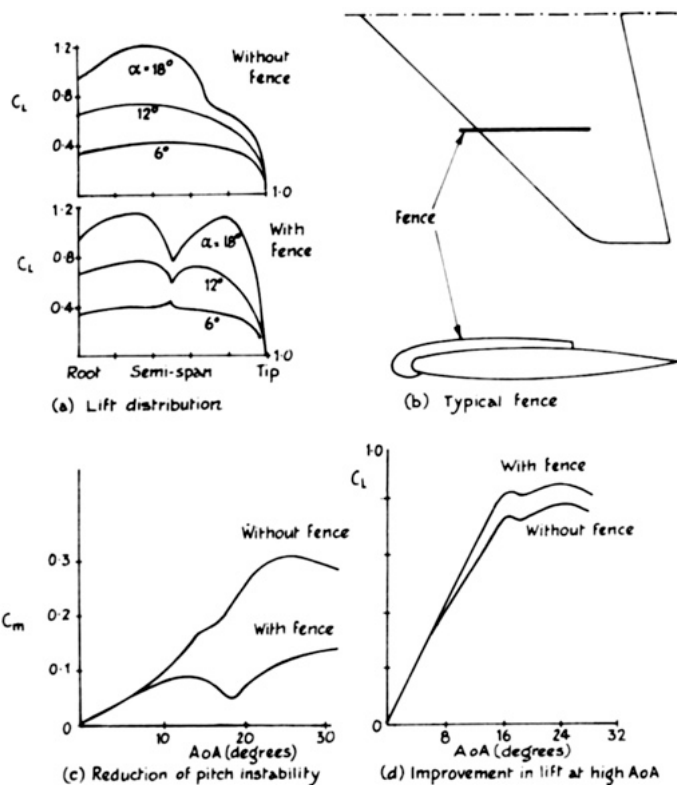
Fences

1. Wing fences are the oldest of the swept-wing palliatives. Early, as many as three per wing half might be seen but now just one per half is more typical.
2. Fences may be designed to act on the boundary layer flow, or the external flow, or both.
3. Fences dam the spanwise flow of air and create flow separation and associated vortices.
4. The inwardly-directed flow created by the vortex near the wing surface retards spanwise BL flow. Outboard, the BL may be energized by influx of high-velocity air.
5. At high- α , the lift created by the vortex or sets of vortices, may itself be significant.

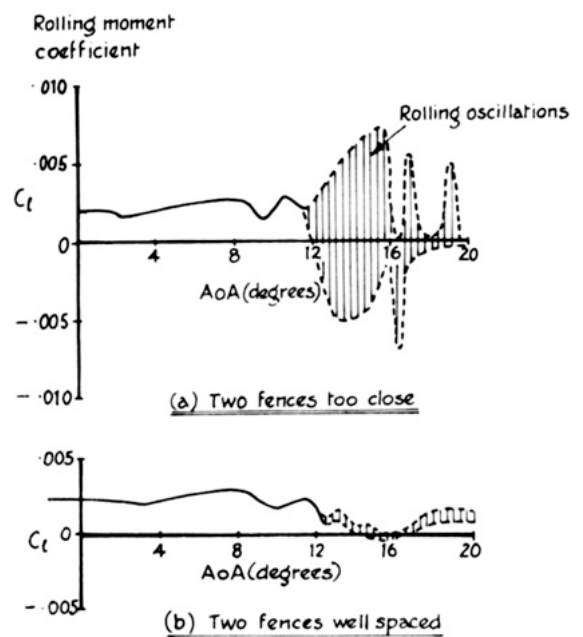


Aerodynamic crutches — 3

Improved aerodynamic performance associated with fences



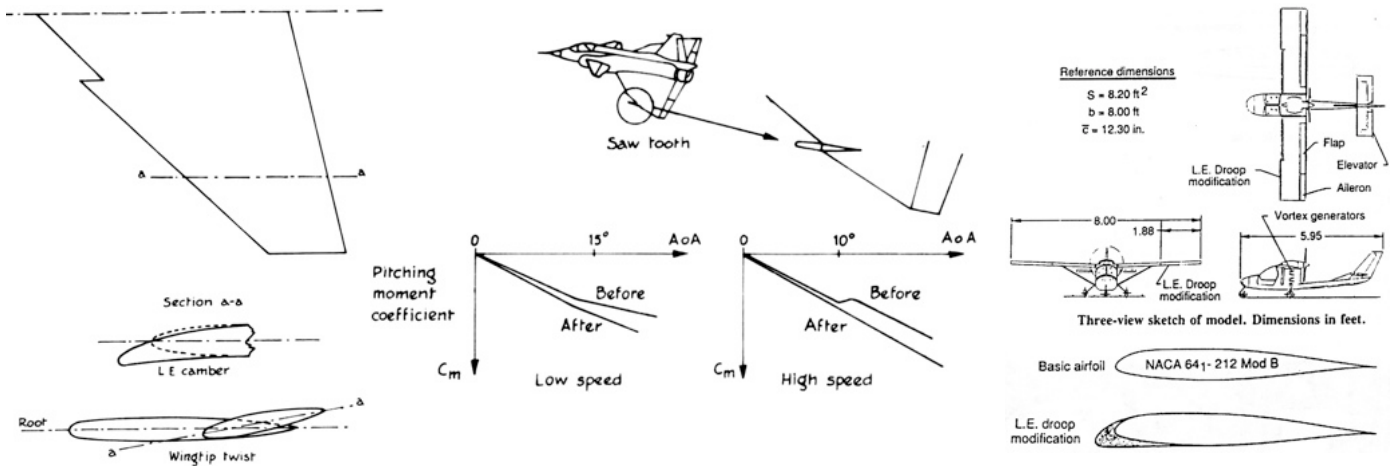
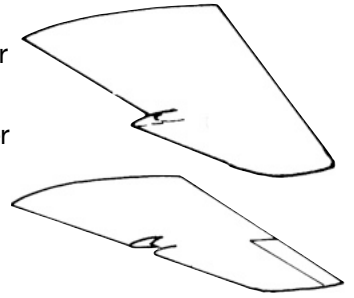
Improved aileron effectiveness/controllability (Harrier)



Aerodynamic crutches — 4

Saw-tooth and notch

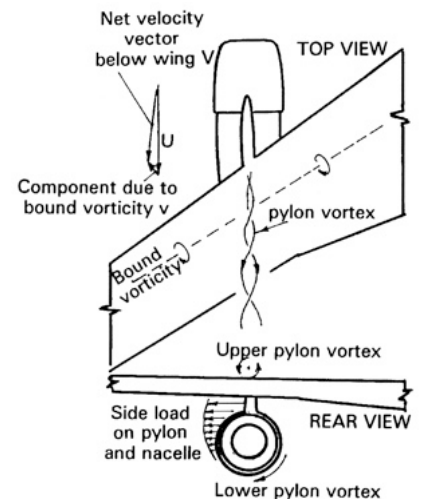
1. Both devices rely on creating trailing vortices with inward-directed flow near the wing surface.
2. The saw-tooth may also be used to introduce LE camber/washout to further improve handling. Also t/c is reduced, lowering supersonic drag.
3. The notch is largely the 'inverse' of the saw-tooth and creates similar flows.
4. The saw-tooth is also used to improve handling on some straight-winged aircraft also.



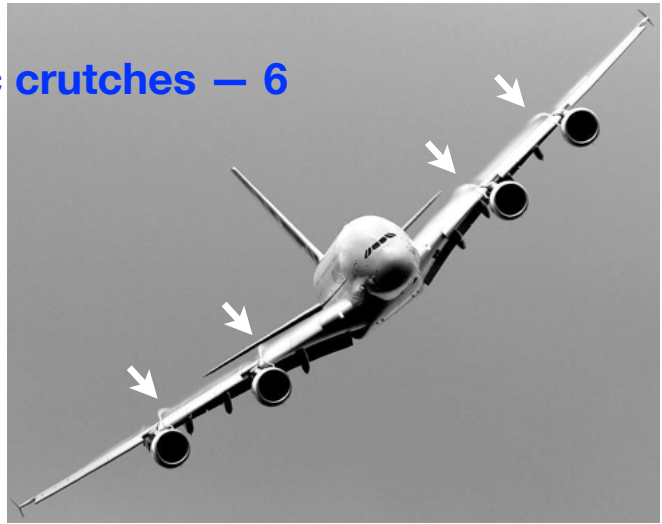
Aerodynamic crutches — 5

Pylons, and engine-mounted devices

1. Pylons for stores and especially engines act like fences to block spanwise flows which are comparatively large on the underside of swept wings, owing to general spanwise BL flow, tip-vortex flows, and interaction with swept bound circulation.
2. At high- α , pylon flows may trail over the top of the wing and create inward flows near the wing surface. In fact they are often designed to do exactly this.
3. To enhance or create such flows for high-bypass engines, now often located near the wing, special fins may be added to engine nacelles to provide intense vortices at high- α .

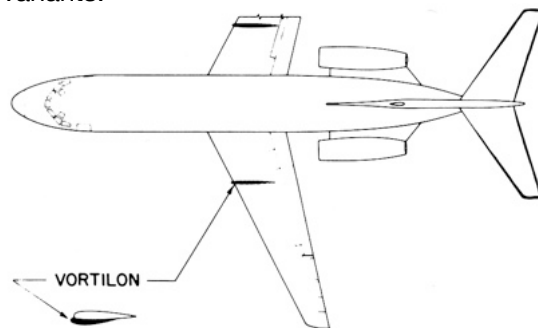


Aerodynamic crutches — 6



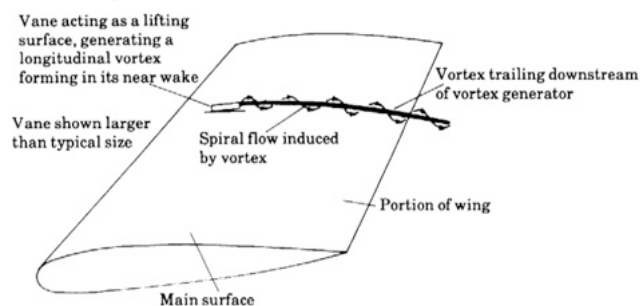
The vortilon

1. The vortilon is in effect a truncated 'fake engine pylon', developed by Douglas to provide similar benefit to that given by under-wing engines.
2. Typically employed on rear-engine aircraft that lack wing-mounted engines. Used by Douglas on early DC-9 variants.



Aerodynamic crutches — 7

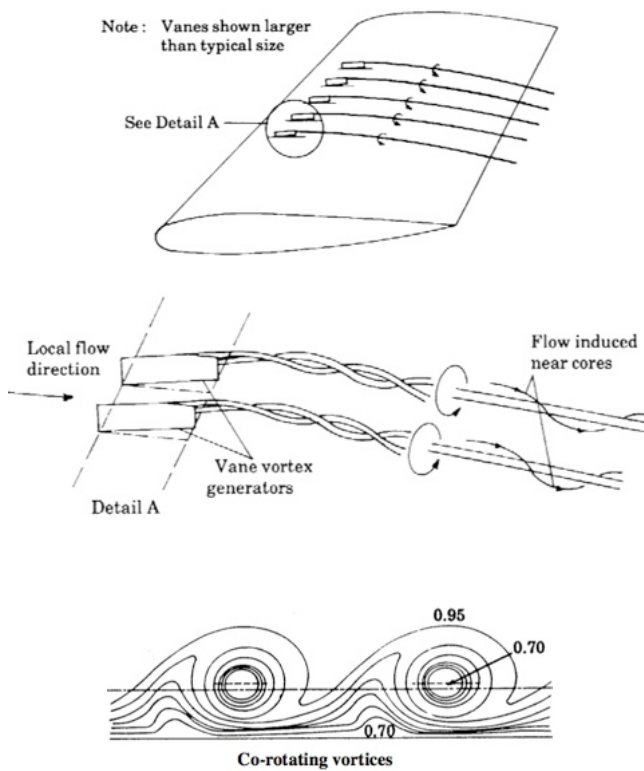
Vane vortex generators



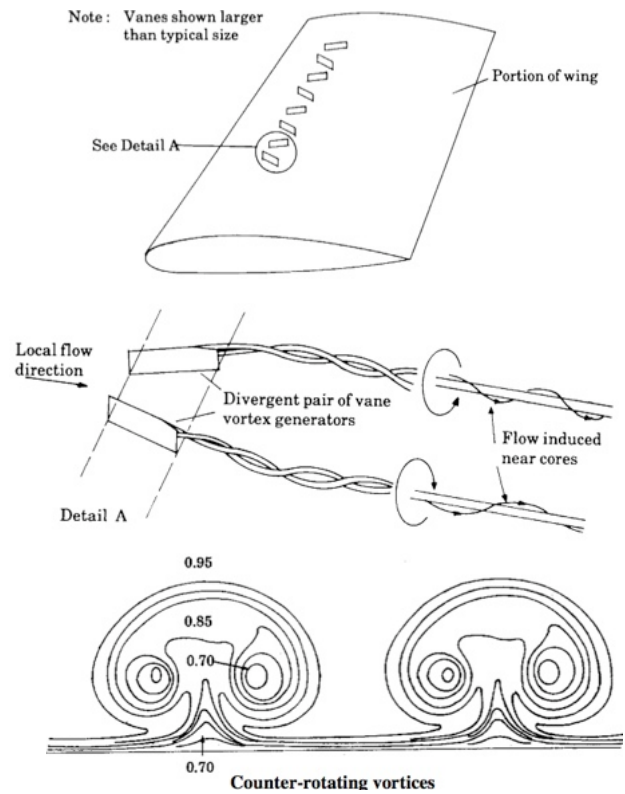
1. Small vanes located in spanwise rows which produce vortices to locally energize BL flow by promoting cross-flow mixing and thereby delay separation.
2. Typically 'co-rotating' or 'counter-rotating' although other arrangements are possible.
3. Counter-rotating types can thin wing BL since fluid is ejected normal to the wing.
4. May be used for subsonic application but often the purpose is to delay shock-induced separation.
5. Generators produce local drag but the overall effect can often be beneficial.
6. Difficult to design without wind tunnel modelling.
7. Not restricted to use on wings.

Aerodynamic crutches — 8

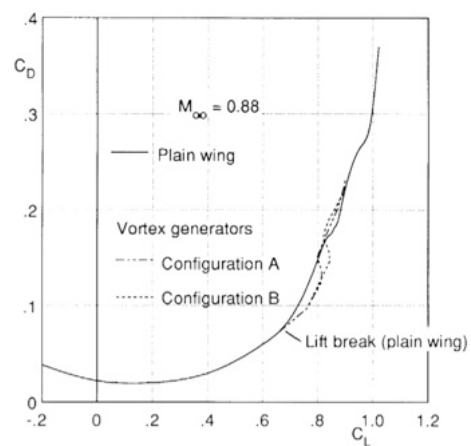
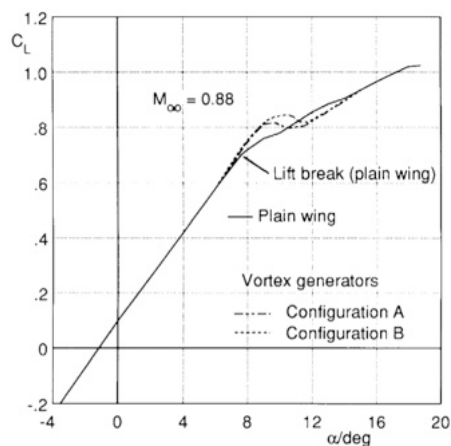
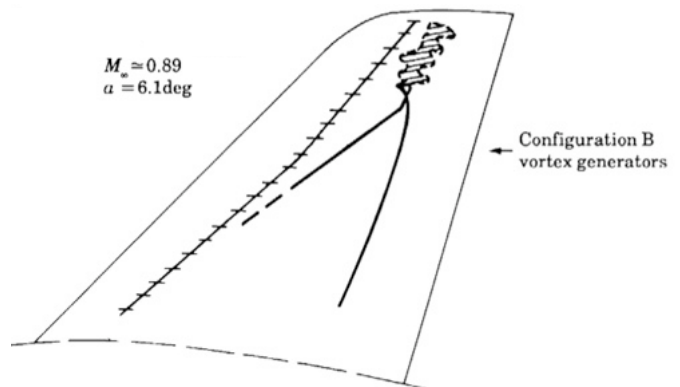
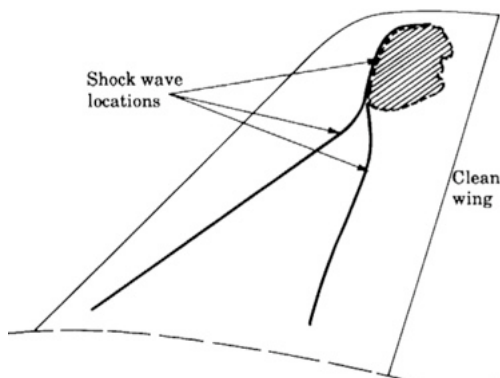
Co-rotating



Counter-rotating



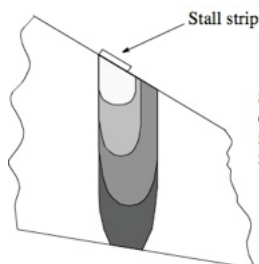
Aerodynamic crutches — 9



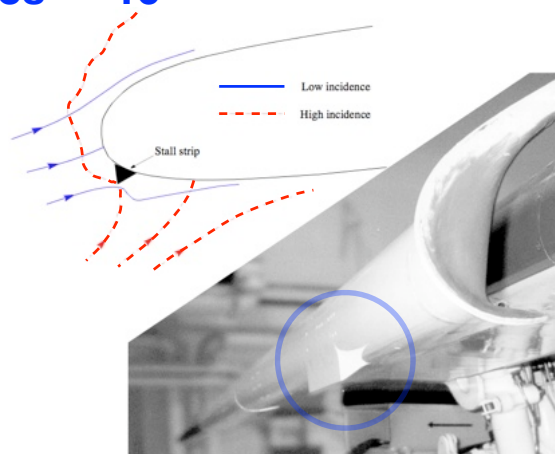
Aerodynamic crutches – 10

Stall strips

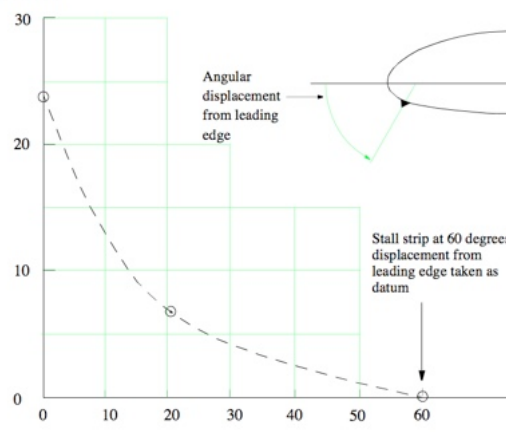
1. Stall strips are designed to promote (relatively) early stall at an inboard spanwise location, and to provide an orderly spread of area influenced by flow separation.
2. Thus they make stalling behaviour more benign and provide the pilot with warning signs such as buffeting.
3. While designed to minimize degradation in C_{Lmax} , stall strips inevitably cause some reduction in peak lift capacity. They have minimal effect at lower C_L .



Shaded areas show regions of upper surface separation increasing with increasing incidence



Percentage reduction in aircraft trimmed, maximum lift coefficient due to location of stall strip



Winglets

1. Winglets are tip extensions which extend the 'trace' of the wing in the Trefftz plane without significantly extending wing span.
2. As a result, for a fixed span, they lower induced drag. However, they also contribute skin friction, profile drag, root bending moment, and weight.
3. A range of studies now suggest that if span is not restricted, it is better to directly increase span (i.e. aspect ratio) than to use winglets to increase the trace length.
4. However, if span is restricted, they are worth considering. Also as a modification to an existing production wing.
5. Generally they make greatest contribution when induced drag is significant, e.g. at high C_L .
6. Also, they are most beneficial on wings/twist distribution that makes the original tips relatively highly loaded.
7. Upper winglets are more beneficial than lower/ split winglets.

